Universidade de Aveiro
Ano 2017

Departamento de Engenharia de Materiais e Cerâmica

Marta Sofia de Pinho Branco

Deposição eletroforética de caulino

Electrophoretic deposition of kaolin

Universidade de Aveiro
Ano 2017

Departamento de Engenharia de Materiais e Cerâmica

Marta Sofia de Pinho Branco

Deposição eletroforética de caulino

Electrophoretic deposition of kaolin

Dissertação apresentada à Universidade de Aveiro para cumprimento dos requisitos necessários à obtenção do grau de Mestre em Engenharia de Materiais, realizada sob a orientação cientifica da Professora Doutora Paula Maria Lousada Silveirinha Vilarinho, Professora Associada do Departamento de Engenharia de Materiais e Cerâmica da Universidade de Aveiro, e da Professora Doutora Maria Elizabete Jorge Vieira da Costa, Professora Auxiliar do Departamento de Engenharia de Materiais e Cerâmica da Universidade de Aveiro.

“Procurar uma resposta, mas as respostas são perguntas mortas. São as perguntas que nos fazem mexer. As certezas fazem-nos parar. As perguntas são a porta da rua. Quando nos interrogamos, quando duvidamos das nossas paredes, é porque estamos a passar pela porta. O facto de nos espantarmos com o que se passa à nossa volta é sinónimo de vida. Os cemitérios estão cheios de pessoas que se espantam com nada.”

Afonso Cruz, em Para onde vão os guarda-chuvas.

O júri

Presidente

Professora Doutora Maria Margarida Tavares Lopes de Almeida

Professora Auxiliar, Universidade de Aveiro

Doutor João Carlos de Castro Abrantes

Professor Adjunto, Instituto Politécnico de Viana do Castelo

Professora Doutora Paula Maria Lousada Silveirinha Vilarinho

Professora Associada, Universidade de Aveiro

Agradecimentos

Agradeço, em primeiro lugar, aos meus pais que são, sem dúvida, o meu pilar e quem mais e, desde sempre, acreditou em mim. Nada, em momento algum, será equiparável ao que sempre fizeram e sei que farão por mim. Seria necessária outra tese para descrever a importância dos meus pais na minha formação académica e pessoal: um enorme e sentido obrigada!

A toda a restante família quero agradecer a paciência pelos momentos de ausência e de menos boa disposição e por terem sempre acreditado que tudo isto era possível.

Um enorme obrigada à Inês que, durante o percurso académico, além de me ter ensinado muito também se tornou uma grande amiga.

João, Diogo, Ricardo Serrazina, Joana, André Santos, André Fonte, Ricardo Silva, Violeta, Rui, Juliana, Celestino e Telha, a todos vocês obrigada pelo constante apoio e amizade. Sei que todos sabem a importância que têm para mim e que tiveram para aqui chegar.

Finalmente, agradeço às orientadoras: Professora Doutora Paula M. Vilarinho e Professora Doutora Elisabete Costa; a todos os colegas no laboratório e a todo o *staff* do DEMaC por toda a disponibilidade, todos os ensinamentos, por todas as sugestões e todas as correções. Agradeço também ao Doutor Igor Bdikin pela realização dos ensaios de nanoindentação, no Centro de Tecnologia Mecânica e Automação (TEMA), no departamento de engenharia mecânica.

Palavras-chave Deposição eletroforética, Caulino, Mulite, Filmes espessos, Orientação de partículas.

Resumo A deposição eletroforética (EPD) é uma técnica interessante do ponto de vista de processamento de materiais permitindo a formação de filmes dos mais variados materiais em diferentes substratos condutores. É uma técnica simples, versátil e de baixo custo associado.

No presente trabalho, conduziram-se estudos que permitiram estabelecer as condições apropriadas para a produção de filmes espessos de caulino por EPD. Depositaram-se filmes de caulino em verde, com cerca de 5 mg, em três tipos de substrato: aço inoxidável, folha de platina e silício platinizado.

Para a identificação das condições de deposição, contribuiu o estudo sistemático das condições de preparação da suspensão de caulino que incluíram a avaliação do potencial zeta de suspensões com o pH da mesma, do efeito da composição do meio suspensor (água, etanol, ou mistura de ambos), do recurso ao iodo como aditivo, e da variação com o tempo da transmitância da luz UV por parte dos diferentes meios suspensores, com ou sem iodo. Os resultados obtidos permitiram concluir que as melhores condições de deposição são as que combinam a adição de alguma água ao etanol, enquanto meio suspensor, e o uso de iodo como aditivo.

Os filmes preparados por EPD foram sinterizados a 1200 e 1300 ^{o}C, durante 2 h.

A microestrutura dos filmes, antes e após sinterização, observada por microscopia eletrónica de varrimento (SEM) permitiu concluir que as partículas de caulino tendem a depositar de uma forma orientada em que as suas superfícies basais se alinham paralelamente ao substrato. Os filmes de caulino sinterizados foram submetidos a ensaios de nanoindentação e determinou-se a sua dureza Vickers e módulo de Young para os quais se obtiveram, respetivamente, 300 MPa e 40 GPa.

Este trabalho contribuiu para identificar condições para obter filmes espessos de caulino de cuja a microestrutura anisotrópica se aponta a possibilidade de aceder a propriedades maximizadas segundo determinadas direções o que do ponto de vista das suas aplicações pode abrir novas oportunidades.

Key words Electrophoretic deposition, Kaolin, Mullite, Thick films, Particles orientation.

Abstract

Electrophoretic deposition (EPD) is an interesting technique from the point of view of materials processing. The technique allows the formation of films of many different materials on different conductive substrates. Besides that, EPD is a simple, versatile and low cost technique.

The studies conducted, in the present work, allowed the establishment of appropriate conditions to produce kaolin thick films by EPD. Green kaolin films with around 5 mg were deposited on three types of substrate: stainless steel, platinum foil and platinized silicon.

A systematic study about the preparation conditions of the kaolin suspension contributed to identify the deposition conditions. This study included the assessment of the pH dependence of zeta potential of the suspension and the effect of the suspension media (water, ethanol or a mixture of both) as well as the use of iodine as additive. Transmittance variation of the UV light with time was also assessed for the different suspension media with and without iodine. The obtained results allowed to conclude that the best deposition conditions are those that combine the use some water in the ethanol based suspension media added also with iodine.

The kaolin films produced by EPD were sintered at 1200 and 1300 ^{o}C for 2 h.

The observation of the films microstructure by scanning electron microscopy (SEM), before and after sintering, allowed to conclude that the kaolin particles tend to deposit in an oriented way in which their basal surfaces align parallel to the substrate. The sintered kaolin films were submitted to nanoindentation tests and their Vickers hardness and Young's modulus was determined as 300 MPa and 40 GPa, respectively.

This work contributed to identify the conditions to obtain kaolin thick films of which the anisotropic microstructure is expected the possibility of assessing maximized properties under certain directions. From the point of view of applications, this can open new possibilities.

Table of contents

Index of figures

Index of tables

List of abbreviations and symbols

BET	Brunauer-Emmett-Teller (adsorption isotherm)
DTA	Differential thermal analysis
E	Young's modulus
E_{IT}	Young's modulus calculated from the nanoindentation parameters
EPD	Electrophoretic deposition
H_{IT}	Indentation hardness
HV_{IT}	Vickers hardness
IEP	Isoelectric point
KB	Sintered kaolin bulk
KB_{1200}	Sintered kaolin bulk at 1200 ^{o}C for 2 h
KB_{1300}	Sintered kaolin bulk at 1300 ^{o}C for 2 h
KF	Sintered kaolin films
KF_{1200}	Sintered kaolin films at 1200 ^{o}C for 2 h
KF_{1300}	Sintered kaolin films at 1300 ^{o}C for 2 h
KGr	Kaolin green films
pzc	Point of zero charge
RIR	Reference intensity ratio method
SEM	Scanning electron microscopy
TGA	Thermogravimetric analysis
XRD	X-ray diffraction
ZP	Zeta potential
ΔT	Transmittance variation

1 Introduction

1.1 Motivation and main goals

Electrophoretic deposition (EPD) is a well known thick film shaping process. EPD is an electric charge driven technique in which charged particles in a suspension are deposited in a conductor electrode under an electric field. The main advantages of this technique are: versatility, short time consuming and low cost. It is possible to coat many different shaped electrodes that can be any conductor material. The versatility of the process is also justified because it is possible to perform EPD to several materials as long as they can be prepared as a stable suspension. The process of EPD requires simple equipment which is an advantage from the point of view of thick film production. This work has the following main objectives:

- To carry on the EPD of kaolin suspensions;
- To exploit the conditions to obtain thick films with anisotropic microstructures of oriented microstructures by EPD of kaolinitic particles;
- To evaluate the texturing effect of particle orientation and its impact on the structural, microstructural and mechanical properties of kaolin thick films.

To accomplish these objectives, kaolin and kaolin suspensions will be prepared and characterized in order to establish the adequate conditions for producing the thick films. Following to the sintering step, kaolin thick films will be analysed in order to assess their structure, microstructure and mechanical properties aiming at establishing a relationship between them. After the sintering process of kaolin, mullite is obtained. This is a very stable ceramic product known for its high resistance. Mullite is highly refractory, resistant and it is expected that its needle shape microstructure accounts for its good mechanical properties.

The preferential orientation of the particles together with the intrinsic properties of mullite should result in good quality thick films with enhanced properties given by the conformation process. Kaolin particles orientation has been mentioned as important in very different fields of application, namely the paper industry, traditional ceramics, chemical and pharmaceutical industries. Mullite properties were also investigated and found to be of interest. Among other properties, mullite presents good mechanical properties, high refractoriness, high resistance to wear and corrosive agents and low thermal expansions. A more extensive insight on the properties and applications of kaolin and mullite will later be developed. None of these studies was found to

be about EPD. This work is an exploratory study where the influence of EPD process on the particles orientation and final mechanical properties is going to be assessed.

The intrinsic advantages of the EPD process together with the evolution of kaolin while sintering and the fact that oriented mullite particles can be obtained by the end of the process are the motivation for this work. Its aim lies on obtaining good quality and resistant mullite coatings obtained by a simple and effective technique that combine the interesting set of properties of mullite with the anisotropic properties given the particles orientation.

1.2 Electrophoretic deposition (EPD)

Electrophoretic deposition (EPD) is an electrochemical coating method with increasing interest that can be applied both for the processing of traditional and advanced materials in large or small scale [1]–[3]. Electrophoresis is the first step of EPD and consists on the movement of charged particles suspended in a liquid (dispersion media) under an applied electric field between two electrodes. During the second step (deposition), a relatively homogeneous and compact film forms by the deposition of charged particles at the opposed charged electrode. EPD may be designated as cathodic or anodic deposition depending on if the particles are positively charged and move towards the cathode or if they are negatively charged and move towards the anode [2] [3]. A schematic EPD cell is represented in Figure 1 in which the blue rectangles represent the electrodes that are immersed in the charged suspension.

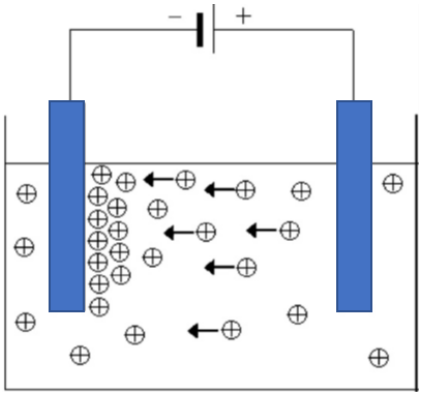

Figure 1 – EPD cell representation showing the movement of suspended positive particles towards the negative electrode (substrate) [2]**.**

The particle size of the powder should be controlled and the suspension should be as free as possible from agglomerates that may originate defects during consolidation. These defects can

be avoided by sedimentation before deposition. Allowing the bigger particles to sediment may eliminate agglomerates hence generating denser films, more homogeneous, with better surface quality, reduced porosity and composed mainly of the smaller particles [1].

After deposition, drying and sintering are required in order to fully densify the deposited film with the corresponding elimination of the porosity and improvement of its mechanical properties [1] [2]. These are critical steps of the process so it is necessary to take some aspects into consideration to improve the final properties and avoid defects. During the drying step, some retraction occurs hence enabling the green body relative density to reach around 60 % while some cracks may appear due to the stress induced by non-uniform shrinkage. During sintering, problems may result from the differences between the thermal expansion coefficients of the substrate and of the deposited film. Another aspect to be considered is related to the nature of the substrate. Usually ceramic films are deposited on metallic electrodes (or other electrically conductive substrate as required for EPD) that may not withstand the high temperatures required to densify some of the ceramic films [1].

Since EPD can be used with different materials and different substrates, sometimes with complex shapes, it is considered a very versatile process. It is also a simple technique with a good cost effectiveness relation because it requires simple equipment and it is short time consuming. Small changes in the electrode shape and positioning allow coating objects with several shapes. Changing parameters such as the deposition time or the applied electrical field allows film properties to be controlled. EPD can be applied to any material in the form of a stable colloidal suspension [1]–[3].

There is no general or universal suspension media for the EPD of oxides [4]. Suspension media used for EPD can be classified in two main groups, aqueous and non-aqueous, in which the most common are acetone, acetylacetone, acetic acid, ethanol, methanol, n-propanol, isopropanol, n-butanol, 2-methoxyethanol, ethylene glycol, tetraethoxysilane, and meth-yltriethoxysilane, with additives that may include acids (hydrochloric and nitric), dopamine, dolapix, hydroquinone, iodine (I_2), nitrocellulose, polyetherimide (PEI), poly(acrylic acid), polyethylene glycol polyvinyl, and pyrrolidone triethanol-amine (TEA), among others [5].

It is possible to use water as dispersive media but most studies related to ceramics and oxide powders are performed using other mediums mainly because the use of water leads to the electrolysis of water and gas release that negatively affects the quality of the coating. If the electrolysis of water is overcome, for example by using low electric fields, aqueous EPD becomes

very advantageous, when compared to organic solvents: water is not toxic, ecofriendly and less expensive [3] [6]. These advantages become very important from the industrial point of view.

1.2.1 Suspension and process parameters

The success of EPD process is highly dependent on the suspension stability and particle electrophoretic mobility (speed of an electrically charged particle when moving in a liquid under an applied electric field). Suspension stability and electrophoretic mobility are influenced by the conductivity of the suspension that results from the interaction of the particles under electrostatic and Van der Waals forces [6]. It is also necessary to ensure good particle dispersion and good control of their surface charge [3].

Particle size between 1 and 20 μm is reported to be suitable for EPD but it is not mandatory. Recently this technique has gained interest for the processing of nanomaterials. Larger particles tend to sediment under the effect of gravity and non-uniform films are deposited with thickness gradients. It is thus crucial that particles are completely dispersed in a stable and homogeneous suspension [3] [7].

Particles in a stable suspension do not sediment or flocculate but if the suspension is too stable the repulsive forces between particles may overcome those exerted by the applied electric field thus preventing the deposition at the electrode [7]. Suspension conductivity is also important because it affects the stability or the particles motion depending on how conductive it is. When conductivity is too high, the particle motion and deposition rate are very low because high conductivities reduce the effective applied electric field on the particles [3] [8]. On the other hand, if conductivity is too low, stability is lost because particles charge electronically [9]. According to Zarbov *et al.* [8], the conductivity should be less than 10 μS/cm [3]. Suspensions with low conductivity and low viscosity are suitable for EPD processes and these parameters may be altered by the addition of electrolytes [6]. The experimental conditions of the EPD process are: the deposition time, the applied voltage, the solids concentration, the nature of the suspension media and the substrate conductivity [3]. Table 1 sums the general effects of each one on the film formation.

Table 1 – General effects of the process parameters on the film formation [3]**.**

Parameter	Evolution of the film
Deposition time	Linear deposition of the film occurs for short periods of time, following the Hamaker's equation (Equation 1) [10], but for higher times the deposition rate starts decreasing.
Applied voltage	The amount of the deposit increases with the increase of applied voltage. Linear deposition of the film occurs for low voltages, following Hamaker's equation (Equation 1) [10], but for higher voltages the deposition rate starts decreasing.
Concentration	Important for multi-component EPD. Concentration should be adjusted to the particles deposition rate.
Substrate conductivity	Low conductivity leads to non-uniform films and slow deposition.

For the same initial powder concentration in the suspension, the film thickness increases as the voltage and time increases. According to Hamaker's equation [10] (Equation 1) the yield of deposition varies linearly with the applied voltage and time.

$$M = \int_0^t aAC\mu E \, dt \qquad \textbf{Equation 1}$$

where M is the mass deposited over time (t), C is the particles concentration, E is the electric field, A is the electrode area, μ is the electrophoretic mobility and a is a coefficient representing the fraction of particles that deposit near the electrode.

The decrease of the deposition rate with increasing deposition time can be explained by the formation of an insulating layer of ceramic particles on the electrode. The amount of the deposit increases with applied voltage but this does not imply a better quality of the deposit. If the applied voltage is too high, it can cause turbulence in the suspension affecting film formation and decreasing the film thickness. With high applied voltage, the particles move faster but they cease to have time to rearrange properly and this prevents the formation of a compact and uniform structure. Solids concentration must be taken into account especially if more than one kind of particles with different depositing rates are used: particles deposit accordingly to their electrophoretic mobility so concentration should be adjusted to allow the desired composition of the film to be obtained taking into account the different deposition rates, thus avoiding compositional heterogeneities [3].

1.2.2 The role of additives on EPD

A high zeta potential (ZP) value in modulus of the suspension to be deposited is one of the key parameters to a successful EPD. ZP is the potential difference between the dispersion media and the stationary layer of fluid attached to the dispersed particle and it is an indicator of the stability of suspensions [8]. High ZP modulus is usually synonym of highly stable suspensions. It can be controlled by using additives such as charging agents (acids or bases), specifically adsorbed ions and polyelectrolytes [8]. ZP values between 25 and 45 mV have been reported as sufficiently high to avoid agglomeration [11]. Many additives may be used to control ZP and the determination of the best additive requires several experimental steps [8]:

- Determination of the effect of cationic and anionic charging agents by plotting ZP *vs* pH curves. These curves should also allow the determination of the best pH working range.
- Suspension conductivity is affected by additives so it should be studied according to the additive concentration.
- Effect of different additive concentrations should be assessed to determine optimal additive concentration.

Generally, these experimental steps are performed by comparison with a standard ZP curve corresponding to the powder suspended in the chosen media without additives [8].

Iodine (I_2) is a widely used additive in EPD systems most of the times with organic suspension media. The combination of these with I_2 usually results in extremely homogeneous and reproducible coatings [11]. A few examples of the use of I_2 as additive for EPD suspensions are listed in Table 2.

Table 2 – Examples of EPD systems where iodine is used as an additive.

Material	Deposition media	Additives	Ref.
Sodium potassium niobate (KNN)	Deionized water	I_2 Sodium dodecyl sulfate	[12]
Yttria-stabilized zirconia (YSZ)	Isopropanol Ethanol Methanol Acetone Acetylacetone Acetone and ethanol mixtures	I_2	[13]–[16]
TiO_2	Acetylacetone Acetone Ethanol Isopropanol Methanol	I_2	[11]
$YBa_2Cu_3O_{7-\delta}$ $Bi_2Sr_2Ca_2Cu_3O_{10+x}$ $Tl_2Ba_{1.6}Sr_{0.4}$ $Ca_2Cu_3O_{10+x}$ $BaTiO_3$	Acetone and water mixtures	I_2	[17]
$BaNd_2Ti_5O_{14}$ (BNT)	Deionized water Glacial acetic acid Acetone Ethanol	I_2	[5]

Vilarinho *et al*. [5] stated that iodine is highly effective in charging BNT powders in acetone suspensions. The powders particles charging occurs according to Equation 2 [5].

$$CH_3CHOHCH_3 + I_2 \rightarrow CH_3CHOICH_3 + H^+ + I^- \quad \textbf{Equation 2}$$

It is suggested that the generated protons are adsorbed on the surface of the suspended particles, making them positively charged and leading to an increase of the electrostatic repulsion forces. The increase of repulsion forces leads to an increase of the ZP of the system. If an excess of I_2 is added, the ZP value tends to decrease due to the presence of an excess of free positive charge. Due to this effect, I_2 is considered a suitable additive capable of increasing the suspension stability which ultimately results in good quality thick films shaped by EPD [5].

Koura *et al.* [17] who worked with various oxides also suggest that H^+ ions are generated in acetone media and later adsorbed to the oxide particles. In the case of Koura's *et al*. work [17], not only I_2 but H_2O is used as additive to the suspension media. Therefore, they propose a slightly different mechanism (Equations 3 and 4) to explain the formation of H^+ protons, resulting from the interaction between acetone, H_2O and I_2:

$$CH_3COCH_3 \overset{H_2O,I_2}{\longleftrightarrow} CH_3C(OH)CH_2 \qquad \textbf{Equation 3}$$

$$CH_3C(OH)CH_2 + I_2 \rightarrow CH_3COCH_2I + H^+ + I^- \qquad \textbf{Equation 4}$$

According to these equations, ions are formed by a self-catalytic reaction in the acetone bath after addition of I_2 and H_2O. Acetone creates an H^+ ion by a keto-enol reaction according to a catalytic action of a coexisting acid or base [17].

Aruna *et al.* [15] performed EPD using mixtures of acetone and ethanol as suspension media. In this work, it was also proposed that the particles become positively charged by adsorption of H^+ protons. The interaction between ethanol and I_2 is described by Equation 5 [15]:

$$CH_3 - CH_2 - OH + I_2 \leftrightarrow ICH_2 - CH_2 - OH + H^+ + I^- \qquad \textbf{Equation 5}$$

ZP values are a good indicator of the stability of the suspension but a high ZP value is not always enough to obtain good EPD conditions. Vilarinho *et al.* [5] reported high (47 mV) ZP values for ethanol based suspensions of $BaNd_2Ti_5O_{14}$ (BNT) suspensions, but continuous deposition was not achieved. Therefore, additional tests such as UV light transmittance, should also be performed to assess the suspension's stability. The previously mentioned ethanol based suspensions showed high values of transmittance (60 %) while the acetone based with I_2 showed lower values (between 10 to 15 %). An ideal suspension to be used in EPD should exhibit a small transmittance and small changes in transmittance over time. This means that the particles stay stable and well dispersed and therefore the suspension has suitable characteristics to be used in EPD [5].

Considering all the mentioned parameters regarding the EPD process, it is perceptible that despite being short time consuming, versatile and cost effective EPD is can also be difficult to control in every aspect. It is thus important to fix most of the variables until a starting point for a first deposition is established and, only after that, to change more parameters and determine their influence on the deposited thick films.

1.3 Kaolinite

A silicate is a silicon oxide based material mainly composed of silicon and oxygen that may present several arrangements of the silicon tetrahedron (SiO_4^{4-}) which is the basic unit of silicates. On a silicon tetrahedron, the silicon atom is at the tetrahedron center and bonded to four oxygen atoms positioned at the tetrahedron corners as represented in Figure 2. Silicon tetrahedra can be arranged as one (1D), two (2D) or three dimensional (3D) structures. One or more of the tetrahedron corner oxygens of silicates can be shared by two silicon tetrahedra on more or less complex structures. When these structures are formed they tend to incorporate cations such as Ca^{2+}, Mg^{2+} and Al^{3+} that may have two functions: compensate the negative charge of SiO_4^{4-} achieving electroneutrality or bond the tetrahedra together [18].

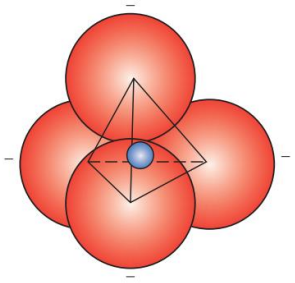

Figure 2 – Silicon tetrahedron representation (red circles represent O and blue one represents Si) [18]**.**

Layered silicates are very common in clays and consist of a sheet or layered structures resulting from the sharing of three oxygen ions in each of the tetrahedra. In this case, electroneutrality is generally obtained due to a second sheet structure with excess of cations that bond to the unbonded oxygens of the first layer. Kaolinite, $Al_2(Si_2O_5)(OH)_4$, is a layered silicate and one of the most common types of clays in which the electroneutrality occurs due to the bonding between $(Si_2O_5)^{2-}$ and $Al_2(OH)_4^{2+}$ layers, as represented in Figure 3. When a series of these double layers are bound parallel to each other, kaolinite crystals are formed occurring as nearly hexagonal flat plates with very small diameters, on the order of the nanometer. Due to its layered structure, kaolinite exhibits plasticity when mixed with water: water molecules fit between the material's layers forming a thin film around the particles acting as a lubricant and permitting them to move over one another [18].

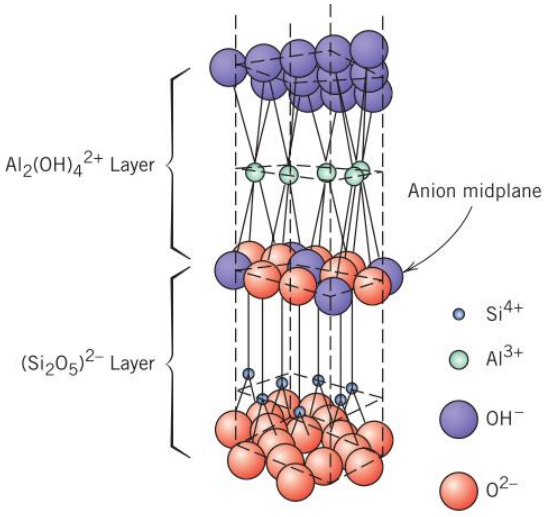

Figure 3 – Kaolinite structure representation [18]**.**

Kaolin is a well-known raw material highly rich in kaolinite and suitable for a wide range of applications due to its white colour, chemical stability in a wide range of pH and high melting point. Kaolin is also nonabrasive and it is an electrical and heat insulator. It is used in paper industry as whitener; in plastic and paint industries as coating and or filler. For these applications, its particle size and colour must be well controlled. Kaolin is also highly used in ceramics industry being porcelain's main component and accounting for its whiteness. This raw material can also be used in refractories. In smaller scale, kaolin is also applied in chemical industry to produce aluminium compounds, fertilizers and pesticides, production of zeolites, and also in pharmaceutical industry [19].

Kaolin particles present lamellar shape with basal surfaces much larger than its edges. Kaolin edges size is below 50 nm [20]. Typical kaolin particle morphology can be observed in Figure 4. It is also visible that particles with very different sizes coexist on the same sample. Kaolin specific surface area ranges are normally between 5 and 25 m^2/g [21]. The particles anisotropy accounts for anisotropic properties of clay bodies thus the orientation of the particles should enhance certain properties on certain directions. A topic on particle orientation and ceramic texture will be briefly discussed afterwards.

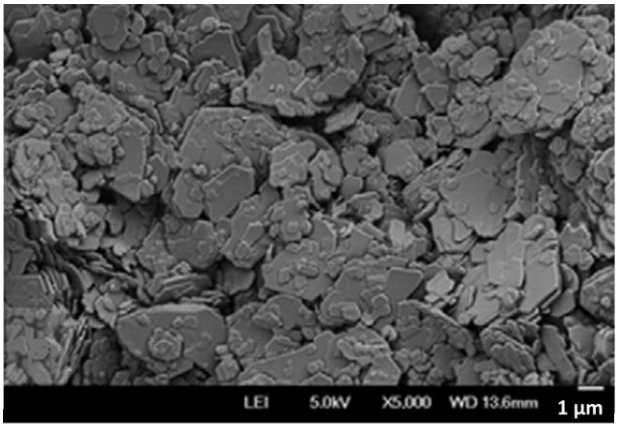

Figure 4 – Micrograph of a kaolinitic sandstone fractured surface showing the typical morphology of kaolin particles [21]**.**

A typical ZP *vs* pH curve of a kaolin in aqueous suspension is presented in Figure 5. It is visible that the value of ZP modulus increases with the increase of pH. According to Pek-Ing *et al.* [22] these results were reproducible for different solids concentrations. In this case, a point of zero ZP was found approximately for pH 3. Despite this, it is common that some kaolinites do not present a point of zero ZP. This is common when the material presents in its constitution one or combinations of the following compounds: CaO, silica, mica and illite [22]. The pH value to which a null value of ZP is obtained is called the point of zero charge (pzc) [20].

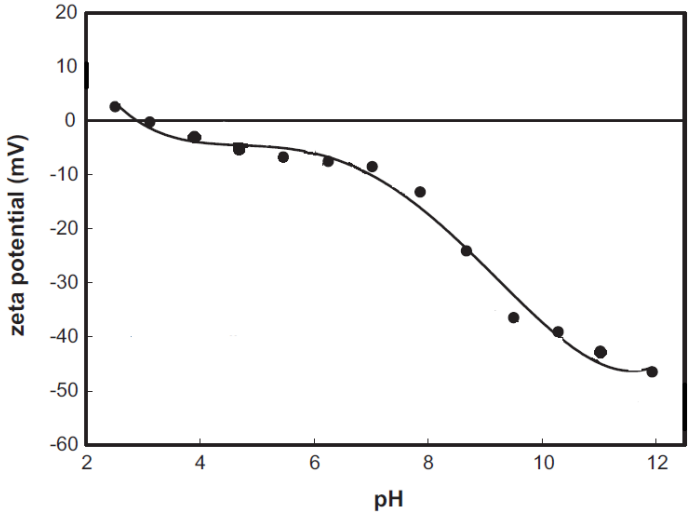

Figure 5 – Typical pH dependence of ZP for a kaolin aqueous suspension. Adapted from [22]**.**

1.3.1 Sintering behaviour and evolution of the mechanical properties of kaolin

Kaolin tends to react with atmospheric moisture when exposed to the air. This combination is reversible and the material loses the physically bonded water at around 300 °C. After this, kaolinite transforms into metakaolinite according to Equation 6, approximately at 600 °C by a dehydroxylation reaction. Both these reactions appear as endothermic peaks in differential thermal analysis (DTA) curves such as presented in Figure 6 [23] [24].

$$2SiO_2.Al_2O_3.2H_2O \rightarrow 2SiO_2.Al_2O_3 + 2H_2O$$ **Equation 6**

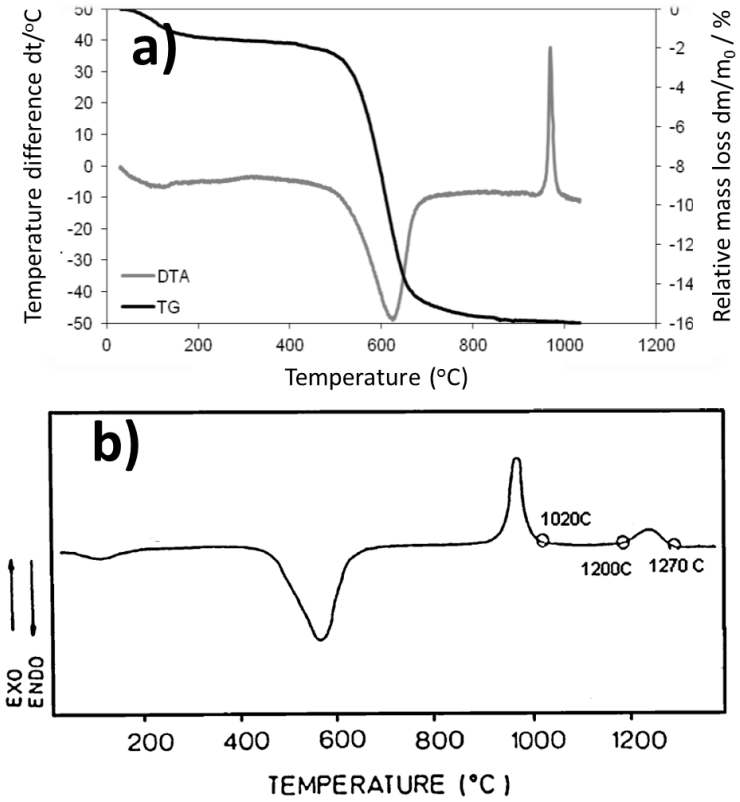

Figure 6 – Typical DTA an TGA curves of a kaolin: a) DTA and TGA curves performed until approximately 1000 °C [23] **and b) DTA curve performed until approximately 1300 °C** [24]**.**

At around 980 °C metakaolinite suffers an exothermic process that is not fully explained yet and two different reactions are proposed (Equations 7 and 8) [23]:

$$2SiO_2.Al_2O_3 \rightarrow SiAl_2O_4 + SiO_2$$ **Equation 7**

$$2SiO_2.Al_2O_3 \rightarrow \gamma Al_2O_3 + 2SiO_2$$ **Equation 8**

In the first case, a spinel ($SiAl_2O_4$) is formed and in the second case the product is γ alumina. Amorphous silica is a product of both the proposed reactions [23]. According to Chakraborty [24], these reactions occur simultaneously and during the crystallization of the spinel phase, traces of weakly crystalline mullite and non-crystallized mullite appear. The spinel phase is latter transformed into mullite and the amorphous silica transforms into cristobalite by exothermic processes at around 1200 °C [24].

Dimensional changes occur during the heating process and they can be quantified by a dilatometry such as the one presented in Figure 7. Regarding these dimensional changes, it can be referred that initially a very small expansion of the material occurs due to the release of physically bonded water. At the same time, thermal expansion and shrinkage occur due to simultaneous heating and water losses. At approximately 550 and until 950 °C, shrinkage is observed which is due to structural water release. After 950 °C, shrinkage still occurs due to the metakaolinite transformation [23].

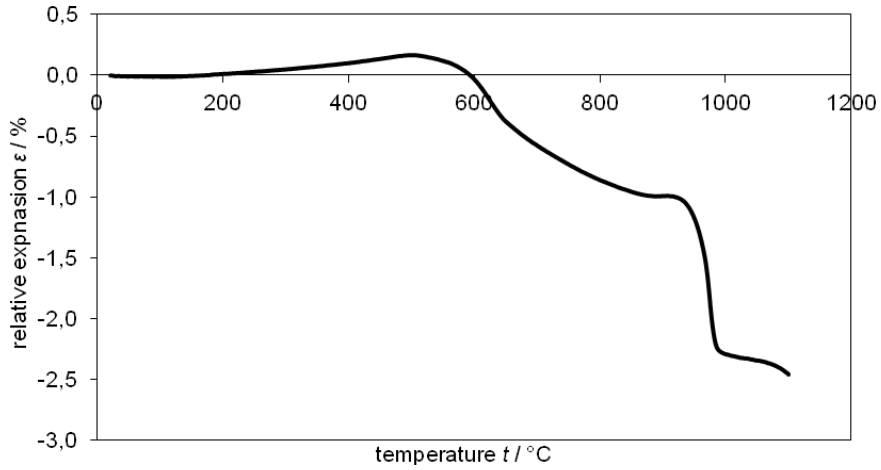

Figure 7 – Typical dilatometry curve of a kaolin [23]**.**

All the mentioned phase transformations imply changes on the material's properties. Stubna *et al.* [23] studied the evolution of kaolin Young's modulus (E). While sintering, *in situ* measurements of the Young's modulus (E) were acquired and the results are presented in Figure 8.

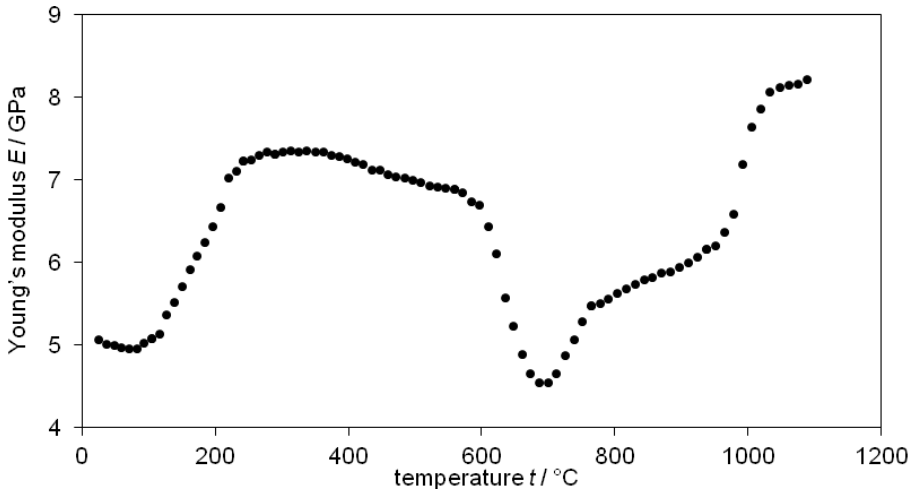

Figure 8 – Evolution of *in situ* kaolin Young's modulus during sintering [23]**.**

As observed, an initial increase of E is noticed until around 300 °C, which reflects the losses of adsorbed water that is a process which leads to the initial densification of the structure. After this, no phase transformation occurs until close to 600 °C. Between 300 and 600 °C, E decreases due to weakening of the interatomic forces since the temperatures are too low for sintering and the previously lost water left an inconsistent structure with porosity. During the dehydroxylation process, starting at around 500 °C, microporosity is formed inside the kaolin crystals which justifies the intense decrease of E until 700 °C. At this point, E starts to increase due to the improvement of the crystal interfaces. Electrically charged defects formed during dehydroxylation and that are mainly located on the crystal surfaces lead to attractive Van der Waals forces formation between metakaolinite crystals that together with the starting of solid state sintering justify the increase of E. From 700 to 970 °C, E increases due to solid state sintering phenomena. At this last temperature, the strong E increase is due to intensive shrinkage and decrease of porosity that occur during the transformation of metakaolin [23].

1.4 Electrophoretic behaviour of clays

Clay particles are usually considered negative due to structural substitution of Si^{4+} for Al^{3+} and for this reason, when dispersed in water, they should move to the positive electrode [6]. This negative charge of clay particles refers only to their basal plane which charge is independent from the pH conditions [20]. A more detailed representation of the surface charge of clay particles is presented in Figure 9, being the basal planes blue and the edges purple. While the basal surfaces are always negative, the charge of the edges depends on the pH. Variations of pH imply different

conditions of attraction and repulsion between clay particles which can affect suspensions stability. When pH is below the pzc, attraction is the dominant interaction among clay particles. On the other hand, repulsion will be dominant when the pH value is above the pzc [20].

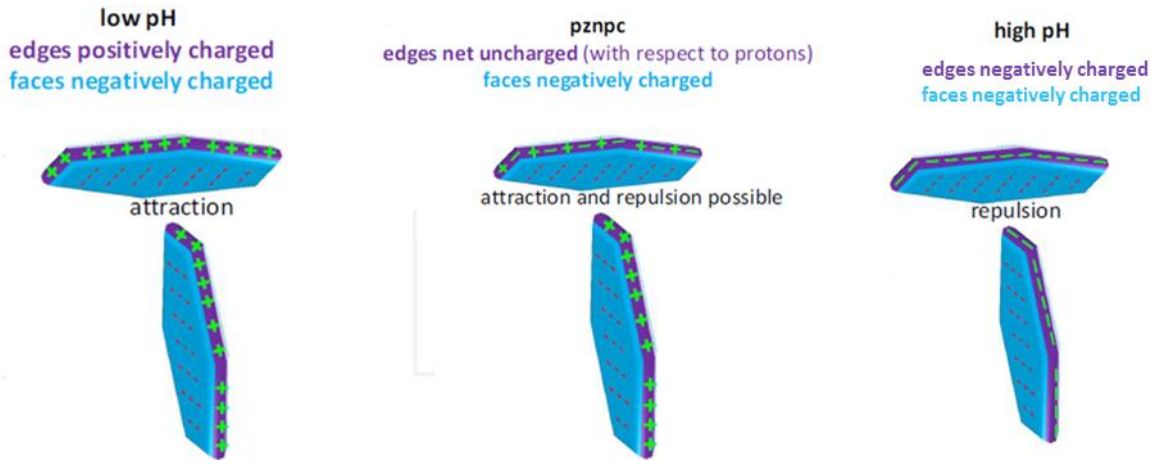

Figure 9 – Representation of the anisotropic surface charge of clay particles. Variation of the edges charge according to pH conditions of the media. Adapted from Preocanin *et al.* [20]**.**

The surrounding dispersive media interacts with the particles and it may take or release protons from hydroxyl groups of clay edge surfaces. The proton exchange depends on the nature of the hydroxyl groups and on the proton concentration on solution. At the pzc, adsorption and desorption of protons does not occur. The pzc is intrinsic to each system and many values can be reported depending on the kind of used clay or clay mineral [20].

The stability of kaolin particles dispersion is influenced by aspects such as the chemistry of the used dispersive media, the particles properties and process conditions (suspension pH, ZP, shear rates and stirring conditions) [25]. Since the stabilization of kaolin suspensions is an important step in many fields of application (ceramics, cosmetics, paints, coatings), many dispersants have been studied: sodium silicate, sodium carbonate, sodium pyrophosphate, sodium salt of poly acrylic acid, polysaccharide based dispersants, etc. [25] [26]. In the case of EPD, having a stable and well dispersed suspension is very important to obtain good deposition conditions and therefore good quality films [1]. Many studies about the stabilization of kaolin suspensions exist but so far none was found on literature for a specific application on the EPD process.

Some EPD water based working systems were reported by Heavens *et al*. [7] and the ones related to clay or clay based materials are presented with the corresponding additives in Table 3, though the available information regarding the additives effect or the suspension media on EPD process is relatively scarce. Nevertheless, this information can be a starting point to the present

study. By analysing the list of additives, it is possible to observe that sodium silicate is nowadays still used, being also mentioned by Piccinini *et al.* [6].

Table 3 – EPD clay based systems reported by Heavens *et al.* [7].

Material	**Additives**
Kaolinite	Na_2CO_3, NaOH, Na_2SiO_3, $Na_2P_4O_7$
Kaolinite, mica, talc, pyrophilite	$Na_2P_4O_7$
Kaolinite, feldspar, quartz	$Na_2P_4O_7$
Kaolinite, illite	$Na_2P_4O_7$
Porcelain	Na_2SiO_3

EPD was proposed by Éntelis *et al.* [27] as a less time consuming shaping process to obtain porcelain bodies using an EPD cell as the one presented in Figure 10. To build this cell, a cup was used to mould copper electrodes which walls were placed equidistantly so that the suspension was under a uniform electric field leading to uniform deposits. Éntelis *et al.* [27] porcelain composition is presented in Table 4 and sodium silicate was used as electrolyte at concentrations between 0.2 and 0.3 wt.% in suspensions with 32 to 34 wt. % of water. The applied voltage and current were varied between 12 and 24 V and 1.25 to 2.50 A, respectively. The deposition time was changed from 30 to 60 s [27]. In this case, EPD moulding was considered a process with easy regulation and good reproducibility of the parameters and therefore considered suitable for the production of porcelain bodies [27]. Despite that, this work did not boost any tendency for producing porcelain by EPD.

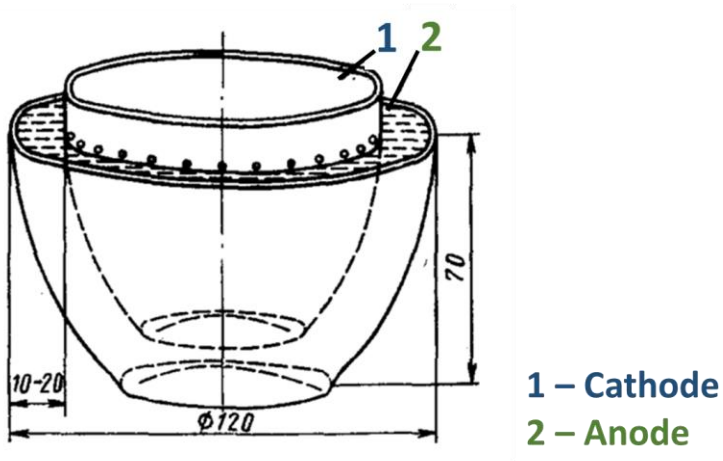

Figure 10 – Representation of an EPD cell used to obtain a porcelain cup. Adapted from [27].

Table 4 –Porcelain composition used by Éntelis *et al.* to shape a cup by EPD [27]**.**

Material	% Weight
Prosyanovsk kaolin	37
Druzhkovsk clay	9
Feldspar	18
Quartz	28
Porcelain waste	8

1.5 Mullite

Despite being rare in natural rocks, mullite is one of the most stable phases developed in both traditional and advanced ceramic products [24] [28]. Mullite can be obtained from raw materials such as alumina combined with silica and from aluminosilicates (sillimanite, andalusite, bauxite, kaolinite, and others). Multiple traditional shaping processes of the green state of clay based materials are possible so it advantageous to use them as raw materials to obtain mullite [28]. Using EPD to shape kaolin is therefore a way to obtain mullite but, in this case, using an advanced and non traditional process. Kaolinitic clay confers plasticity to green bodies while shaping and promotes mullite formation during sintering [29]. Depending on its particle size and amount, mullite accounts for the following properties of the materials [24] [28]:

- High refractoriness and thermal shock resistance;
- High thermal stability;
- Low thermal expansion;
- High resistance to spalling
- High resistance to corrosive agents;
- Increase of the rigidness due to elongated needle shaped crystals.

Mullite may exist in ceramics of many different shapes that can range from very large refractory products to small engineering components of high purity and homogeneity. Polycrystalline mullite products can be divided into three main categories as shown in Table 5 [28].

Table 5 - Main categories of mullite ceramics and respective applications [28]

Mullite category	Applications
Monolithic ceramics	Tableware; Porcelain; Construction and engineering ceramics Refractories and kiln furniture; Substrates for catalytic convertors; Electronic devices; Optically translucent ceramics for high temperature furnace windows.
Coatings	Environmental barrier coatings for furnace tubes and heat shield of space re-entry vehicles.
Mullite matrix composites	Components and structures for gas turbine engines; High duty kiln furniture; Burner tubes; Heat shield of space re-entry vehicles.

Mullite is a solid solution in which various ratios between Al and Si are possible. It may be represented by the following chemical formula: $Al_{4+2x}Si_{2-2x}O_{10-x}$ ($0.2 < x < 0.9$ which corresponds to 55 to 90 mol % of $Al2O_3$) [28]. Besides having several possible ratios between Al_2O_3 and SiO_2, several foreign cations can be incorporated on its structure [28]. Some general properties of mullite are summed in Table 6.

Table 6 – Main physical properties of mullite [28] [30]**.**

Density (g/cm^3)		2.8 – 3.2
Water absorption (%)		0
Modulus of elasticity (GPa)		150
Melting point (°C)		1880
Thermal conductivity (kcal m^{-1} h^{-1} °C^{-1})	**20 °C**	6
	1400 °C	3

Mullite properties are intrinsically related with its microstructure. Mechanical properties, for example, are dependent on the type of mullite that is formed. It is thus interesting to understand the under which circumstances each type of mullite is formed. Three different types of mullite microstructures are known and they are represented in Figure 11. These types of mullite can appear simultaneously [29]:

- Primary mullite (type I) - cuboidal crystals that form at lower temperatures;

- Secondary mullite (type II) – elongated needle-shaped crystals that form later in the firing process. Its aspect ratio is 3-10:1;
- Secondary mullite needles (type III) – needles with higher aspect ratio (30 – 40:1) that form when surrounded by more fluid environment that enhances grain growth.

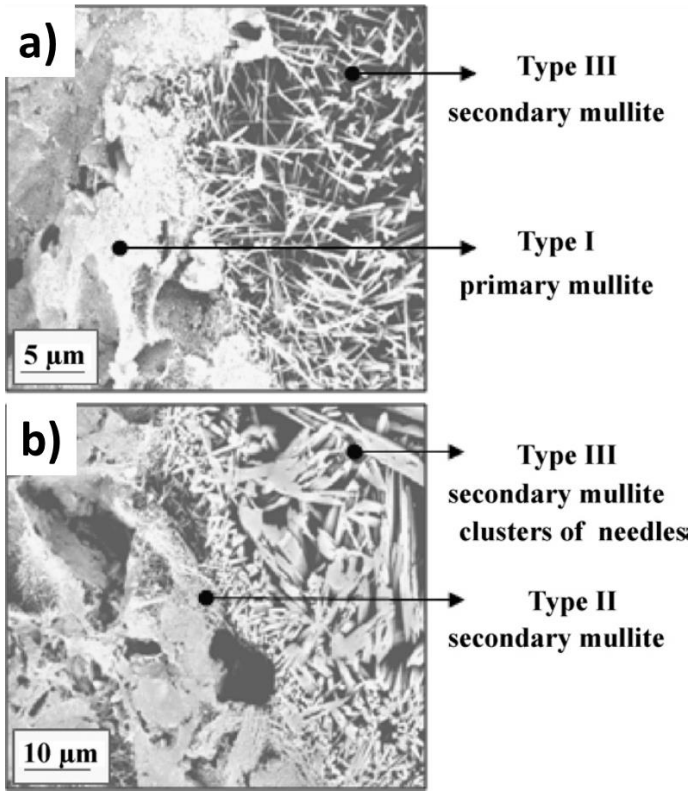

Figure 11 – Possibilities for mullite microstructures: a) Type I (cuboidal crystals) and Type III (needles with high aspect ratio) and b) Type II (elongated needle-shaped crystals) and Type III [29]**.**

The temperature interval for the formation of mullite types I and II ranges between 1200 and 1400 ^{o}C. The surrounding environment is also a key aspect regarding the type of mullite is formed. At higher temperatures within the referred interval, type II is more likely to be formed. For higher aspect ratio and for the occurrence of type III mullite, a lower viscosity surrounding medium is required. For type III to be formed, the temperature interval is between 1250 and 1400 ^{o}C [29]. Enhanced strength and toughness is achieved when a high aspect ratio mullite is present in porcelains [29] [31].

1.6 Particle orientation and ceramic texture

Kaolin is largely used in paper industry because it has platy small sized particles that allow coatings with good gloss and printability. The effect of kaolin particles orientation in water based functional coatings for paperboard was studied by Rissa *et al.* [32] who showed that the coating gloss is affected by the particles orientation and the pigment composition. An increase on the kaolin content of the pigment leads to an increase of both the particles orientation (parallel to the coating surface) and the gloss values [32].

Preferential orientation of kaolinite particles was reported by Boussois *et al*. [33] to improve the toughness and strength of a silicate ceramic. Microstructural arrangement is highly influent on the material's mechanical properties: the higher the microstructural organization the better the mechanical properties [34]. Preferential orientation of anisotropic grains can be induced by shaping processes such as tape casting, centrifugation, pressing, etc. [33] [35].

EPD of kaolin is going to be performed aiming to obtain films with oriented particles for exploring their properties and potential applications. Anisotropic properties may be maximized by assessing those properties on ceramics with oriented grains.

Clay minerals with layered structures have anisotropic properties due to its crystals plate shape that are formed under natural sedimentation and consolidation conditions that affect crystal orientation and pore size distribution [36]. Antal *et al*. [36] studied the influence of texture in illite and kaolin based materials shaped by hand moulding and extrusion and found that extruded kaolin bodies have a higher tendency than illite to develop texture, although additional studies were mentioned to be required. Texture is important to be addressed since it may lead to anisotropy of mechanical, thermophysical and electrical properties of thin ceramic bodies. In the case of Antal *et al*. [36] work, regarding to kaolin samples (see Figure 12) it was demonstrated that:

- Material's crystal texture was confirmed by X-ray diffraction (XRD) analysis.
- Material's retraction during sintering is more significant in the transversal direction relative to the processing direction.
- Young's modulus present significant differences when assessed in the axial or transversal directions: samples with transversal texture present lower Young's modulus than samples with axial texture.

Axial and transversal directions of Antal *et al*. [36] samples are schematically represented in Figure 12 and are relative to the processing conditions.

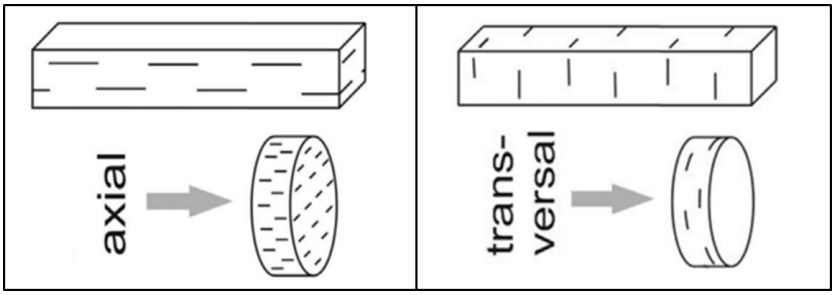

Figure 12 – Representation of axial and transversal texture of Antal's [36] **samples obtained according to the processing direction. Axial and transversal directions are relative to the basal planes of the clay particles.**

2 Methods and materials

2.1 Kaolin films and bulks fabrication

Kaolin films were produced by EPD using the deposition cell represented in Figure 13. The conductive substrates were placed between parts 1 and 2 and covered with a polymeric mask with a 10 mm diameter opening that defines the deposition area. The distance between the electrodes is 20 mm.

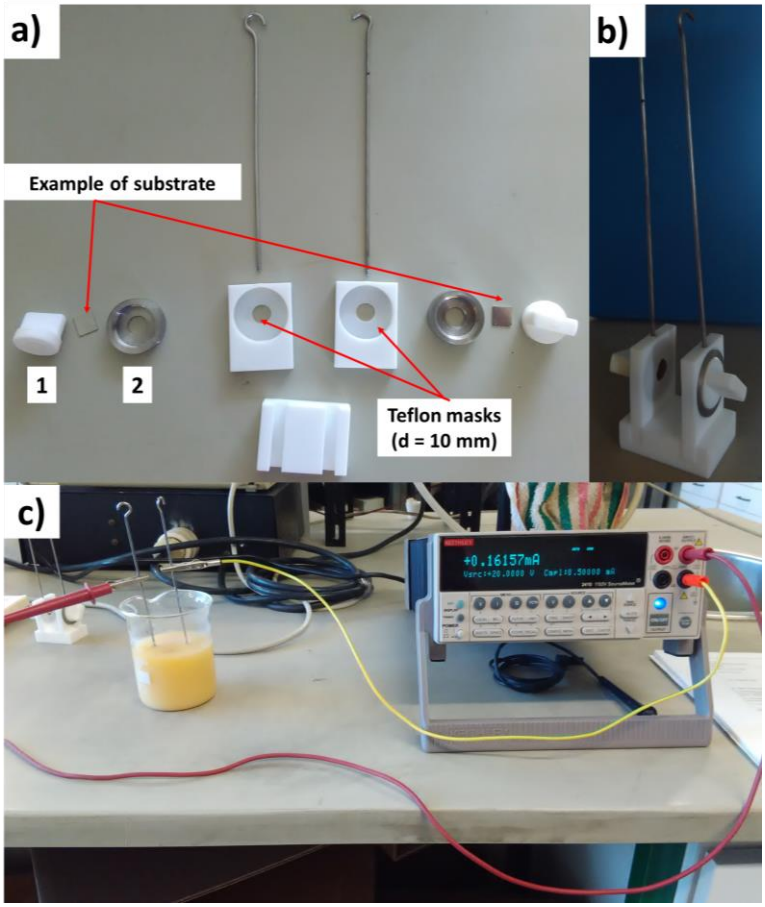

Figure 13 – Home made EPD apparatus used in this work: a) unassembled cell; b) assembled cell and c) cell immersed on the suspension and connected to the electrical source.

Stainless steel substrates (*0.5 x 10 x 10 mm, AISI 316 Foil, Goodfellow, UK*) were used both as electrode and counter electrode. Due to oxidation problems during the sintering step, a second batch of films was deposited using platinum reused foil (*11 x 11 x 0.025 mm, Goodfellow, UK*) as

electrode and stainless steel substrate as counter electrode. Under the same conditions, a third batch of films was deposited on platinized silicon substrates. These films were used to assess the mechanical properties of the sintered films. Before the depositions, the substrates were rinsed with water and then ultrasonicated in ethanol during 10 min so that stains and grease could be removed. Green films weight was calculated by the difference between the weight of the substrate before and after deposition.

Kaolin powders (10 g/l of suspension) were suspended in a solution of ethanol (absolute anhydrous, *Carlo Erba, 99.999 % v/v*) and deionized water (0.9 χ_{mol} ethanol + 0.1 χ_{mol} water) and then added with 1 wt.% of iodine (I_2) (*Merck, 99.999 %).* Prior to the addition of iodine to the suspension, a saturated ethanolic solution of I_2 was prepared from which a volume (corresponding to 1 wt.% of the mass of solids in the suspension) was added to the kaolin suspension using a micropipette. The EPD cell was placed together with the suspension in a glass container and a *KEITHLEY 2410* electrical source was used to perform the depositions at 20 V during 15 min. Once prepared and before starting the EPD, the suspension was ultrasonicated for 45 min followed by magnetic stirring for 45 min.

After deposition, the films were dried at room temperature for at least 48 h and then sintered in a box furnace at 1200 and 1300 ^{o}C for 2 h with a 10 ^{o}C/min heating and cooling rate. Since the furnace has no ventilation, the cooling rate beyond a certain temperature (~ 400 ^{o}C) could not be controlled being therefore a natural cooling rate of the furnace.

To produce kaolin bulk samples, kaolin powders were uniaxially pressed at 125 MPa for 1 min and isostatically pressed at 245 MPa for 15 min. A 10 mm diameter die was used to shape the pellets. After pressing, the pellets were sintered together with films under the same sintering conditions.

The nomenclature defined for the various kaolin samples under analysis is presented in Table 7.

Table 7 – Nomenclature of the different kaolin samples under study.

Material	Nomenclature
Kaolin green films	KGr
Sintered kaolin films	KF
Sintered kaolin films at 1200 °C for 2 h	KF_{1200}
Sintered kaolin films at 1300 °C for 2 h	KF_{1300}
Sintered kaolin bulk	KB
Sintered kaolin bulk at 1200 °C for 2 h	KB_{1200}
Sintered kaolin bulk at 1300 °C for 2 h	KB_{1300}

2.2 Powder, suspensions, films and bulk characterization

2.2.1 X-ray diffraction (XRD)

X-rays are electromagnetic waves with wavelength between 0.01 and 1 nm. In the case of XRD technique, x-rays are produced by the interaction of a high-energy electron with the target surface. When x-rays interact with an atom, it starts to behave as a secondary source of electromagnetic waves. Therefore, the atom starts to behave as a dispersion point emitting x-rays in every direction. From this point, interactions between electromagnetic waves start to occur and minimum or maximum of intensity are obtained when the interactions are destructive or constructive, respectively. According to Bragg's law, only favourably oriented atomic plans relatively to the incident radiation lead to constructive interferences and consequently to a diffraction point [37]. Bragg's law is described by Equation 9,

$$2dsen\theta = n\lambda$$ **Equation 9**

where d is the interplanar spacing (Å), θ is the angle between the incident beam and the diffraction planes from the crystal lattice, n is a positive integer and λ is the incident radiation wavelength.

XRD was used to identify the crystalline phases of kaolin powders, bulk and films. A *Panalytical – X'Pert-PRO* X-ray diffractometer was used. The analyses were performed at room temperature, with a target source of X-ray of copper, in which the wavelength of the radiation $K_{\alpha1}$ and $K_{\alpha2}$ are 1,54060 and 1,54443 Å, respectively. The scan range started at 2θ = 5.0066 until 2θ = 79.9906. The angle step size and the scanning step time were 0,0130 ° and 198.6450 s, respectively.

Reference intensity ratio (RIR) method was applied for phase quantification to complement the technique, using Equation 10 [38],

$$\chi_{\alpha}^{m} = \frac{(I_{hkl})_{\alpha}^{m}}{RIR_{\alpha}} \left[\frac{1}{\sum_{i}^{n} \frac{(I_{hkl})_{i}^{m}}{RIR_{i}}} \right] \qquad \textbf{Equation 10}$$

where χ_{α}^{m} is the mass fraction of the α phase, $(I_{hkl})_{\alpha}^{m}$ is the integral intensity of the peak with higher diffraction intensity of α phase, RIR_{α} is the RIR parameter of the α phase that corresponds to the I/I_C value that can be found on the *powder diffraction file* (PDF) of the phase, $(I_{hkl})_{i}^{m}$ is the integral intensity of the peak from *i* phase and RIR_i is the corresponding RIR parameter [38].

2.2.2 Morphology and microstructure observation

Scanning electron microscopy (SEM) is a powerful technique to observe the surfaces of the materials allowing ranges of magnification up to 50 000 times, thus enabling microstructures to be characterized. In this technique, the surface to be examined is scanned with an electron beam. A reflected electron beam is later collected and displayed on a cathode ray tube producing an image that represents the surface features. This technique can be complemented with extra equipment so that localized qualitative and semiquantitative elemental analysis can be obtained [18].

SEM (*Hitachi S-4100* equipment) was used to observe the kaolin powders particles morphology (shape and size) and the microstructures of KGr, KF and KB samples. All the produced films and bulks were observed in both top view and cross section directions, except KGr because they could not be cut without damage since they were very delicate on the green state. When trying to cut this samples, the powders always ended up loose from the substrate. In some cases, *ImageJ software* was used to assist the analysis of the obtained micrographs. For powder particles SEM analysis, a piece of carbon conductive tape (*Ted Pella, INC*) was glued to a SEM sample holder and the powders scattered on it from a spatula. The excess of powders was removed with compressed air. To cut the KF a diamond pen and a ruler were used to draw a clean cut over the ceramic part. After being cut, the films were placed in the SEM sample holder with carbon conductive tape as shown in Figure 14.

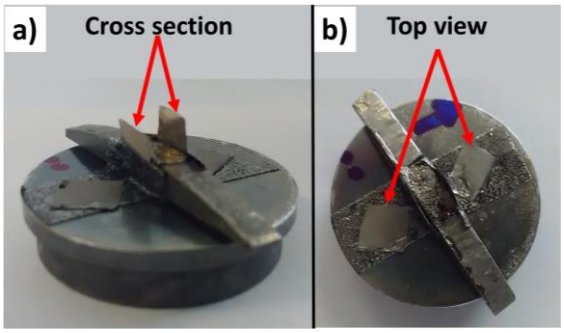

Figure 14 – Positioning of KF samples to be observes in SEM: a) samples placed at 90 ° relative to the sample holder for cross section observation; b) samples parallel to the sample holder for top view observation.

In the case of KB, cross sections were observed using both the polished and fracture surfaces. A specific sample preparation was required before SEM observation. KB samples were cut and impregnated in araldite resin as shown in Figure 15. For the impregnation with araldite, a *Calfofix Kit* was used and a mixture of 20 parts (wt.) of resin to 6 parts (wt.) of hardener was prepared. The mixture was poured into a plastic mould where the KB samples were placed with the desired surfaces facing down. After being cured at 70 ^{o}C for 5 h, the araldite holders were removed from the plastic moulds and then the surface was polished. SiC abrasive papers and diamond pastes were used. To reveal the grain boundaries, a chemical etching with fluoridric acid (5 vol. % with deionized water) was performed during 1 min.

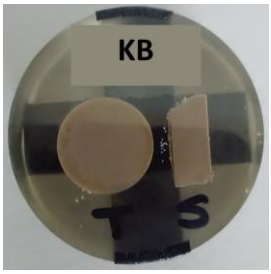

Figure 15 - Positioning of KB samples on araldite supports to be observed in SEM. Araldite holder is glued with conductive carbon duct tape to the SEM sample holder.

Regarding the KB fracture surface, the samples were simply cut using a plier and then glued with conducting carbon cement (*Leit-C*) to the SEM sample holder.

It was necessary to perform a carbon deposition on the top of all the samples so that the surfaces became electrically conductive. A *K950X Turbo Evaporator* was used.

The surface morphology (top view) of the prepared KGr and KF films was also assessed with a *Leica EZ4HD* optical magnifier.

ImageJ is an image edition software that also allows measurements on the images. It was, in this case, used to perform the measurements of the thickness of kaolin particles edges. After the establishment of the appropriate scale on the software, line by line measurements were made and the data was statistically analysed.

2.2.3 Thermal analysis

Thermal analyses were used to study the chemical and physical reactions of kaolin with temperature. These reactions were determined by assessing the endothermic and exothermic events and weight variations that occur during a thermal cycle imposed to kaolin. For differential thermal analysis (DTA) and thermogravimetric analysis (TGA) a *Linseis Adidi 40* equipment was used. The analyses were run from room temperature until 1200 ^{o}C under a heating rate of 10 ^{o}C/min. DTA output is the temperature difference between the sample under analysis and a reference sample. This output may evidence endothermic or exothermic peaks. Endothermic peaks can be associated with losses of water and carbonates decomposition, for example. On the other hand, exothermic peaks can be associated with organics combustion and crystallization or recrystallization reactions, for example. TGA is frequently performed at the same time as DTA and allows to detect the mass change of the sample during the heating processes [39].

Dilatometry is used to measure expansion or shrinkage of materials while heating. During the analysis, the sample is placed in a movable furnace and a pushrod is placed against the sample to transmit the length change [39]. Using a *BAHR Dil 801L* dilatometer, a dilatometry was also performed in order to detect dimensional changes of kaolin samples and to predict the kaolin sintering behaviour. In this case, the heating rate was also 10 ^{o}C/min until 1300 ^{o}C. The difference between the maximum temperatures of both analyses is due to different equipment temperature limit ranges. For dilatometry, a pellet was prepared by uniaxial pressing (125 MPa) of kaolin powders during 1 min.

2.2.4 Suspension stability qualitative tests

The stability of kaolin suspensions with different additives was assessed. A kaolin suspension in deionized water (10 g/l) was prepared. After being ultrasonicated and magnetically stirred, the suspension was poured into test tubes to which 1 to 7 drops of a I_2 ethanolic solution, Dolapix and Na_2SiO_3 (*Quimialmel R200/47*) were added. The effect of the different additives was

evaluated in a qualitative way by photographing the suspension ate the moment of the addition of the different additives and later on, after 24 h of resting.

2.2.5 Zeta potential (ZP) analysis

According to the electrical double layer model, the ZP is the potential difference between the dispersion medium and the stationary layer of fluid attached to the dispersed particle, being therefore an indicator of the stability of suspensions. The higher the value of ZP in modulus, the higher the repulsion between particles bearing the same ZP which implies higher suspension stability [40].

A *Malvern Zetasizer Nano ZS* equipment was used to perform the ZP tests to be used as indicators of the suspensions stability. These tests were carried on various suspensions either under the variation of the suspension pH or under the variation of the additive amount (weight of additive per weight of solids in suspension). To perform these tests, suspensions of kaolin (0.4 g/l) were prepared in deionized water and in ethanol.

To measure the pH dependence of ZP (ZP *vs* pH curves), NaCl and HCl solutions were added to kaolin suspensions to respectively increase or decrease the suspension's pH. NaCl and HCl were added drop by drop so that pH variations were approximately 1 between each measurement. To measure the amount of additive dependence of ZP (ZP *vs* amount of additive curves), solutions of 0.04 g/l of each additive were prepared and added to the kaolin suspensions using a micropipette so that known volumes of additive solution were added between each ZP measurement. Dolapix, Na_2SiO_3 (0.04 g/l aqueous solutions) and I_2 (0.04 g/l ethanolic solution) were the tested additives.

2.2.6 Transmittance spectrophotometry

Spectrophotometry is based on Beer-Lambert law, expressed by Equation 11,

$$log_{10}\left(\frac{I_0}{I}\right) = kl \qquad \textbf{Equation 11}$$

where I_0 is the intensity of the incident light, I is the intensity of transmitted light, l is the length of the light-path in the spectrophotometer cuvette and k is a constant for the medium. This law states that "the fraction of light absorbed by a transparent medium is independent of the incident light intensity, and each successive layer of the medium absorbs an equal fraction of the light passing through it" [41].

(I_0/I) is also called absorbance (A) and k is equal to Ɛc where Ɛ is the molar absorption coefficient and c is the concentration of the absorbing species. Therefore, Equation 11 can be rewritten as Equation 12 [41],

$$\Delta A = \Delta \mathcal{E} c l \qquad \textbf{Equation 12}$$

where ΔA is the difference in absorption for the absorbing species.

(I/I_0) is designated as transmittance (T) usually expressed as a percentage. The relation between absorbance and transmittance is given by Equation 13 [41].

$$A = log_{10}\left(\frac{1}{T}\right) \qquad \textbf{Equation 13}$$

Suspension transmittance of UV light was another method for assessing the stability of the suspensions using a *SHIMADZU UV-3100* spectrophotometer. A first test was run on a suspension of kaolin in deionized water of 0.2 g/l to obtain a transmittance spectrum and determine at which wavelength the minimum of transmittance occurs. Successively changing the wavelength of monochromatic light and recording the change of light transmittance by the suspension allows a spectrum to be obtained. Transmittance was measured every 10 seconds during 15 min on kaolin suspensions with different media: deionized water, ethanol, water and ethanol mixture (with and without iodine). For these tests, a wavelength of 1295 nm was used.

2.2.7 Particle size analysis by laser diffraction

In this technique, particle size distributions are determined by measuring the angular variation in intensity of the scattered light as a laser beam passes through the sample. The scattered light angle is inversely proportional to the particle size. After analysing the scattering intensity data, the particle size is reported as a volume equivalent sphere diameter [42]. Kaolin powders particle size distribution was analysed by laser diffraction using a *Coulter LS230* equipment.

2.2.8 Brunauer-Emmett-Teller (BET) surface area analysis

This technique relies on Brunauer, Emmett and Teller (BET) adsorption isotherm theory that describes the physical adsorption of gas molecules on a surface at a constant temperature on the particle surface. It is a popular method used to determine the surface area of porous or finely

divided materials. The determination of the surface area requires two stages. First: determination of the monolayer capacity (number of adsorbed molecules required to occupy all surface sites). Second: calculation of the specific surface area from the value of the monolayer capacity which requires previous knowledge of the average area occupied by each adsorbed molecule, in this case N_2 molecule [43].

Kaolin powders specific surface area was assessed by gas adsoption using a *QUANTACHROME Autosorb IQ2* equipment. The first analysis degasification time was 24 h and a second analysis was performed with 48 h of degasification. In both analysis, the temperature of degasification was 100 ^{o}C and N_2 was used as adsorbent gas.

2.2.9 Mechanical properties

The nanoindentation technique is based on Oliver & Pharr method [44] that is commonly used to characterize small-scale mechanical properties being suitable for determination of films properties. During an indentation, the resistance of a material to a deformation (caused by a constant compressing load from the indenter) is measured. From this method, it is possible to assess the hardness and the elastic modulus of a material by analysing the force *vs* displacement curves that are obtained during a loading and unloading cycle. Nanoindentation is a very local measurement technique and this can be limitation of its use. For heterogenous materials, very different behaviour can be observed on the same sample. It is likely that measurements can be made either on the grain or on the grain boundary of the material. To avoid this, several measurements should be done in order to ensure the statistical meaning of the data [44].

During the indentation tests, the variation of applied force *vs* displacement is measured and graphically expressed (indentation curves). A typical indentation curve for a generic material is represented in Figure 16.

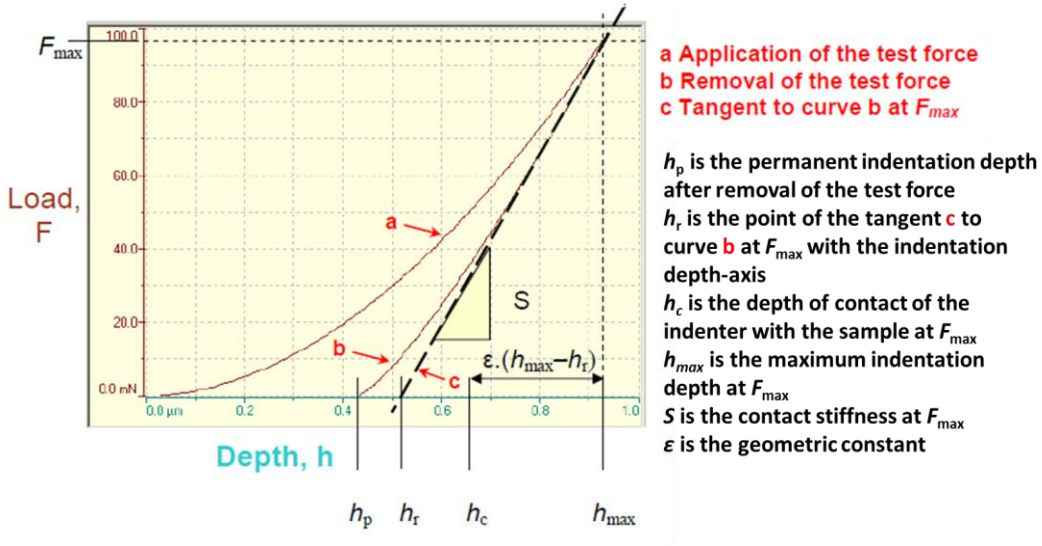

Figure 16 – Typical indentation curve for a generic material, obtained during each indentation test [45].

From indentation curves, it was possible to calculate the indentation hardness (H_{IT}) and the indentation modulus (E_{IT}). H_{IT} is given by Equation 14,

$$H_{IT} = \frac{F_{max}}{A_p} \qquad \textbf{Equation 14}$$

where F_{max} is the maximum force and A_p is the projected contact area.

It is possible to convert it to Vickers hardness (HV_{IT}) using Equation 15 [45].

$$HV_{IT} = \frac{H_{IT}}{10.8} \qquad \textbf{Equation 15}$$

E_{IT} is given by Equation 16, which is equivalent to the slope of the dashed black line in Figure 16 [45],

$$E_{IT} = \frac{1-\upsilon_s{}^2}{\frac{1}{E_r}-\frac{1-\upsilon_i{}^2}{E_i}} \qquad \textbf{Equation 16}$$

where E_i is the elastic modulus of the indenter, E_r is Reduced modulus of the indentation contact, υ_i is the Poisson's ratio of the indenter and υ_s is the Poisson's ratio of the sample.

KF and KB were submitted to nanoindentation tests using an *Indentation tester, CSM Instruments* with a Berkovich indenter. On each sample, indentations were made on a 3 x 3 indentation matrix and the distance between each indentation was 50 µm. The applied forces, on each indentation, ranged between 0.5 and 100 mN.

3 Results and discussion

3.1 Kaolin characterization

It is very important to keep in mind that there are several types of kaolin. This is a natural material mined all over the world and each deposit has its own set of mineral impurities, chemical, mineralogic and morphologic particularities [22]. Typical behaviour and characteristics of kaolin were presented in the first chapter and some discrepancies between the presented data may appear in this section due to the variable chemical and structural nature of this raw material.

The kaolin used in the present work is going to be characterized in this section. Its XRD pattern is presented in Figure 17. Kaolinite, muscovite and quartz peaks were identified and the most intense peaks correspond to kaolinite. As previously mentioned, this technique was complimented with RIR method to quantify the crystalline phases. Phase quantification is presented in Table 8. These results show, as expected, that the kaolin is mainly constituted of kaolinite. Since kaolin is a natural raw material, it is common that not only kaolinite but other minerals are present hence the presence of quartz and muscovite.

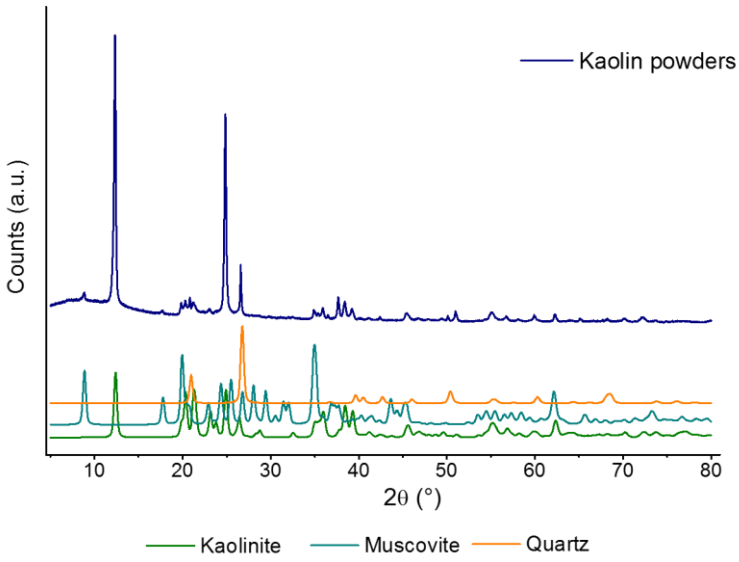

Figure 17 - XRD pattern of the kaolin powders used in the present work.

Table 8 - Mineralogical composition (%) of kaolin calculated by RIR method.

Phase	Quantity (%)
Kaolinite	86.8
Muscovite	6.9
Quartz	6.3

Kaolin powders particles were observed by SEM and the obtained micrographs are represented in Figures 18 and 19. In Figure 18, the typical lamellar shape of the particles is very well evidenced. It is possible to see that kaolin particles tend to form agglomerates of different sizes with the basal planes of the particles facing each other.

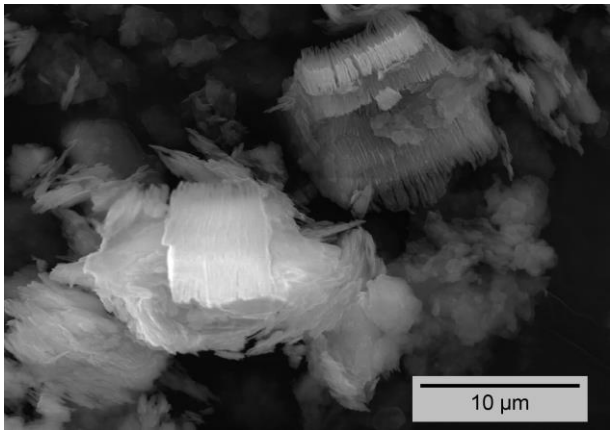

Figure 18 – SEM micrograph of kaolin powders showing the lamellar shape of the kaolin particles.

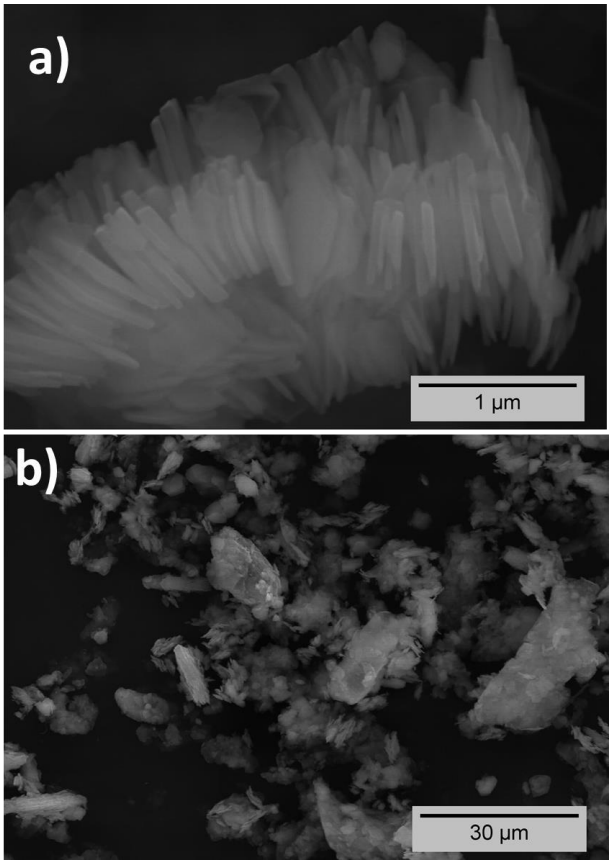

Figure 19 – SEM micrographs of kaolin powders: a) particle agglomerate showing the particles edges; b) overview of the agglomeration state of the particles.

From Figure 19 a) and using *ImageJ* an estimative of the particle edge width was made and the correspondent results are in Table 9.

Table 9 – Average width of kaolin particles edges calculated using ImageJ.

Average edge width (nm)	Minimum value (nm)	Maximum value (nm)	Standard deviation
69	23	128	26

Kaolin particle size distribution is represented in Figure 20. As observed, it is a bimodal distribution evidencing two peaks which denote the average particle size values of 6.8 and 20.7 µm.

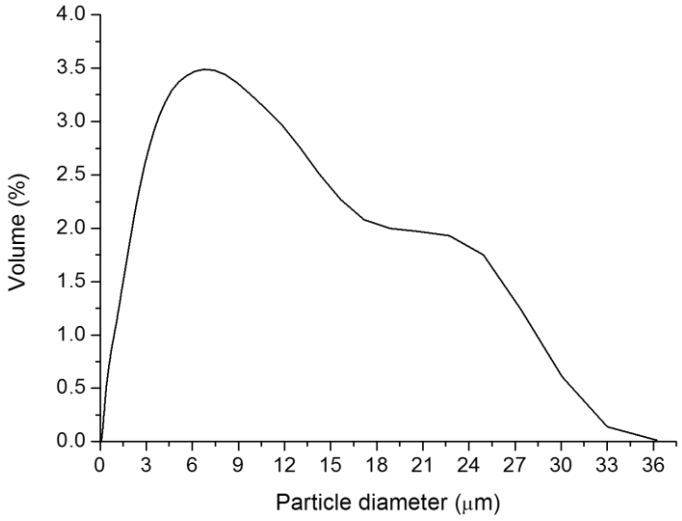

Figure 20 – Kaolin particle size distribution obtained by laser diffraction.

The kaolin particles specific surface area measured by gas adsorption is presented in Table 10. Two measurements were performed to validate the results accuracy. The degasification times and temperature were 24 and 48 h and 100 °C for the first and the second tests, respectively.

Table 10 – Specific surface area of kaolin particles measured under different degasification times and respective correlation coefficients.

Specific surface area experiment	Surface area (m^2/g)	Correlation coefficient
1st run	9.7 ± 0.3	0.99
2nd run	8.6 ± 0.5	0.98

The results of particle size distribution, gas adsorption and the SEM micrographs complement each other. The fact that the particle size distribution is given by a bimodal distribution curve confirms that on kaolin samples often occurs the coexistence of individual particles and or particle agglomerates with different sizes. Particles of different sizes are also visible in Figure 19 b). The same was observed for example on Pruett *et al.* [21] work. Since the particle size analysis by laser diffraction results are based on a volume equivalent sphere diameter these results are only indicative since kaolin particles are far from spherical as confirmed by the SEM micrographs. The particle size distribution values should be considered as the order of magnitude of the particle size for the basal planes. In the case of the particle edge, the average width is 69 nm which is a slightly higher value than the one reported by Preocanin *et al.* [20] that states that the width of the kaolin

particle edges is bellow 50 nm. Since the particles are highly agolmerated, the width measurments could be affected and the real edge width is propably lower than 69 nm. Regarding the surface area, in both analysis the reported value is close to 9 m^2/g which is comprehended in the interval of 5 and 25 m^2/g reported by Pruett *et al.* [21].

The behaviour of kaolin powders suspended in a liquid media needs to be monitored as EPD will be used. ZP curves of kaolin in aqueous and ethanolic suspensions as a function of pH are represented in Figure 21.

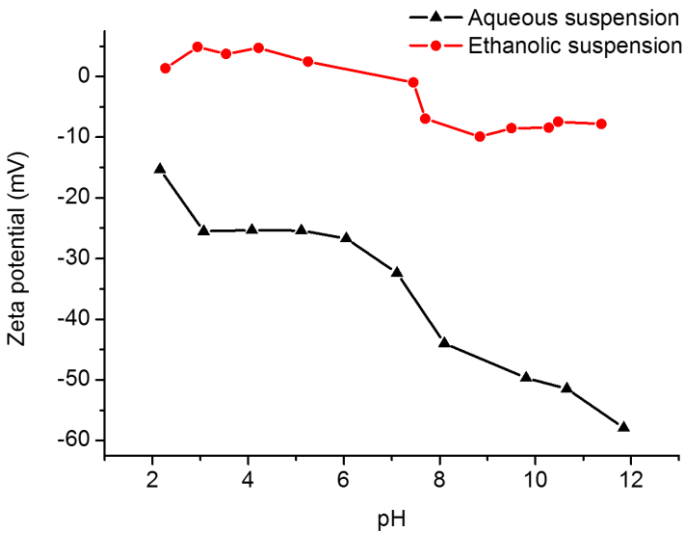

Figure 21 – ZP *vs* pH curves of kaolin in aqueous and ethanolic suspensions.

For both the aqueous and the ethanolic suspensions there is a tendency for the ZP modulus to increase as the pH increases. This behaviour is particularly evidenced for the aqueous suspension. The ZP curve of the present kaolin in aqueous suspension is different from the one of Pek-Ing *et al.* [22] work. The main differences are: the ZP value at pH 2 is negative (approximately -15 mV) and there is no pzc for the studied kaolin in the studied pH range. Observing the XRD pattern in Figure 17, it is possible to see that quartz is part of this kaolin. Since quartz is a form of silica, its presence can justify the absence of the point of zero ZP also according to Pek-Ing *et al.* [22]. For the ethanolic suspension no data was found on the literature for comparison purposes.

Thermal analyses were performed to identify the thermal reactions occurring during heating and to predict the sintering behaviour of the material. In Figure 22 it is possible to observe the DTA/TG curves of the material and in Figure 23 its dilatometry analysis.

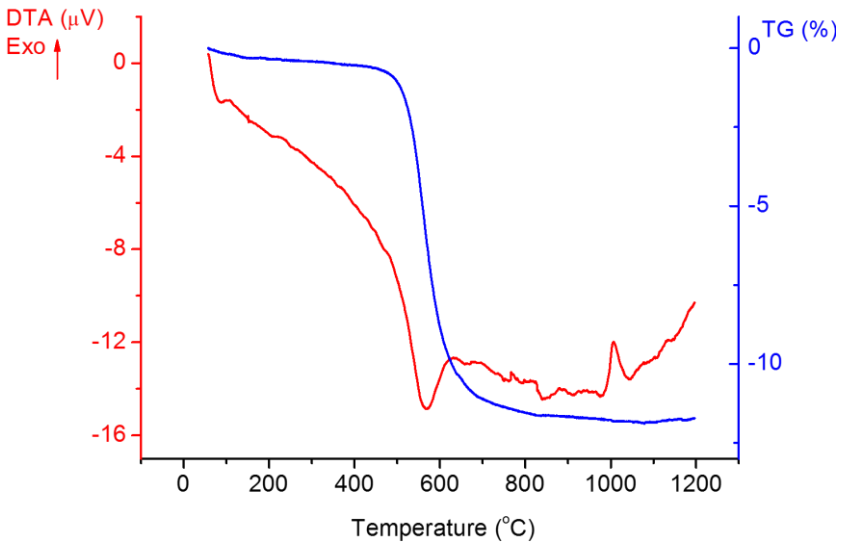

Figure 22 – Thermal analyses of kaolin: the red curve represents the DTA analysis and the blue curve represents the TGA analysis.

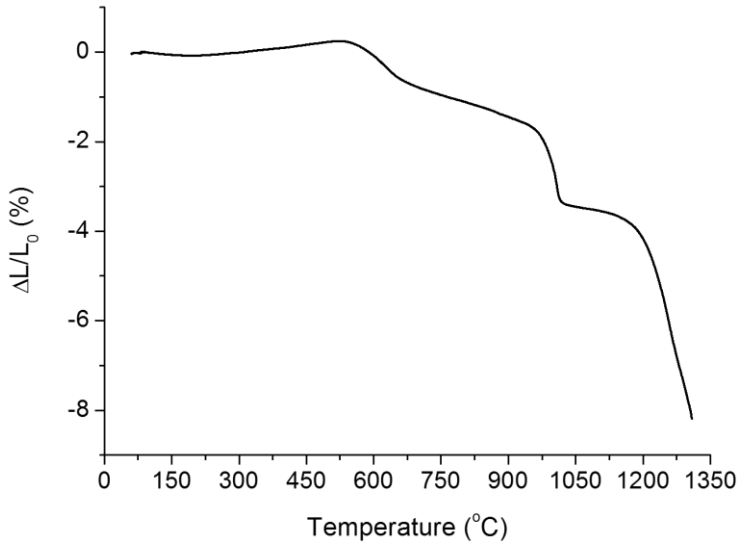

Figure 23 – Kaolin dilatometry: variation of the length (%) of a kaolin pellet with the increase of temperature.

In Figure 22, it is possible to see that at the beginning of the test some mass loss occurs accompanied by an endothermic peak. This happens due to losses of superficial and adsorbed water until around 300 °C. The loss of structural water and formation of metakaolinite is confirmed by weight loss of around 12 % and an intense endothermic peak at around 550 °C. An exothermic peak that accounts for the transformation of the metakaolinite phase is also observed above 1000 °C. Despite some small differences in the recorded temperatures and weight loss such as the endothermic peak at around 550 °C and the less 2 % of weight retraction, the phenomena is quite

similar to the one presented by Stubna *et al.* [23] which indicates that this is a typical thermal profile of a kaolin raw material.

Regarding the dilatometry curve presented in Figure 23, it is possible to see that expansion of the material occurs at the beginning due to the release of surficial water. This curve is not very accentuated because contraction of the pores sites that had water occurs simultaneously. After this, at around 500 ^{o}C the dehydroxylation causes a significant shrinkage of the material. The later transformation of metakaolinite accounts a significant shrinkage step at around 1000 ^{o}C followed then by a shrinkage step starting at 1200 ^{o}C which corresponds to the material densification. In Figure 23 it is also possible to observe that the kaolin's dilatometry presents similarities to that of Figure 7 which corresponds to the work of Stubna *et al.* [23].

As already referred, Figure 23 indicates that the densification of kaolin starts at 1200 ^{o}C. This was chosen as the first sintering temperature because it is the lowest temperature of the interval of temperatures at which mullite starts to form, according to J. Martín-Márquez *et al.* [29]. This interval extends to 1400 ^{o}C but the dilatometry was not performed up to such temperature. Another batch of samples were sintered at 1300 ^{o}C aiming a higher densification of the material and thus better mechanical properties. At higher temperatures, type III mullite is expected to crystallize and thus enhance the mechanical properties [29].

3.2 Characterization of kaolin suspensions

Na_2SiO_3 and Dolapix are commonly referred on the literature as stabilizers for kaolin suspensions [26] being also used in the industry. Even though these additives have not been mentioned for the EPD process, some trials were performed using these additives. Initially, a simple test was performed to assess qualitatively the stability of kaolin suspensions using these additives. Since iodine is widely used in EPD processes (see Table 2), it was also tested. The kaolin suspensions were prepared as described before and different amounts of the additives were added to different test tubes. The effect of these additives can be observed in Figures 24, 25 and 26.

In Figure 24, it is visible that adding 1, 3 or 5 drops of Na_2SiO_3 results in stable suspensions even after 24 h. These suspensions have small portions of transparent supernatant solutions and small amounts of kaolin sediment at the bottom. When more than 5 drops of Na_2SiO_3 are added, the volume of transparent supernatant solution increases as well as the sediment. Even though there are no visible differences on the photo between test tubes S_0 and S_1, the kaolin sediment on the bottom of test tube S_0 (where no Na_2SiO_3 was added), was slightly bigger than the one on test

tube S_1. This shows that kaolin aqueous suspensions are stable even without additives but the stability can be improved with small amounts of additive.

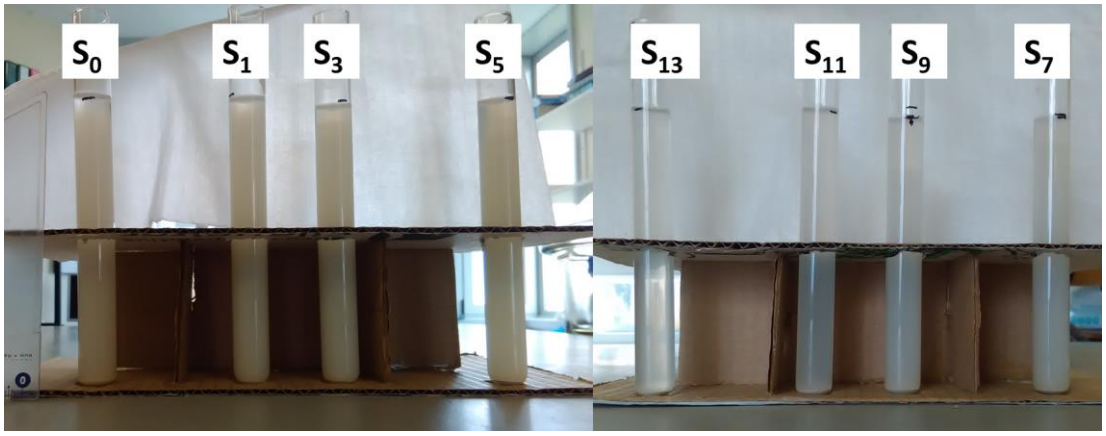

Figure 24 - Effect of the addition of 0 to 7 drops of Na_2SiO_3 to kaolin aqueous suspension after resting for 24 h. The label S_n means that "n" drops of Na_2SiO_3 were added to the kaolin suspension.

In Figure 25, it is possible to observe that after 24 h the suspension to which 1 drop of dolapix was added (D_1) showed a small amount of transparent supernatant and a small amount of kaolin sediment at the bottom. As the amount of dolapix increased (D_2 to D_4), the supernatant became bigger. It can thus be concluded that a small amount of Dolapix stabilizes the kaolin aqueous suspension even after a long period of resting (24 h).

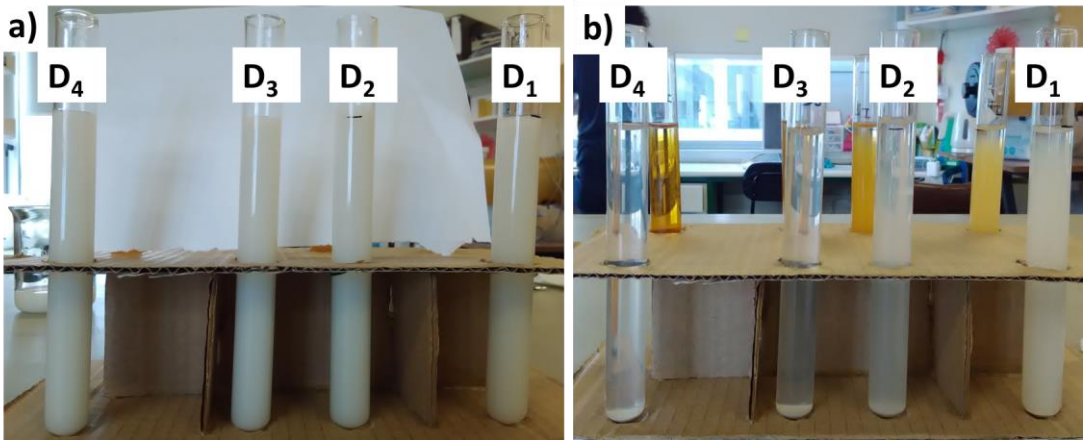

Figure 25 - Effect of the addition of Dolapix to kaolin aqueous suspension: a) immediately after addition of 1, 2, 3 and 4 drops; and b) after 24 h of resting. The label D_n means that "n" drops of Dolapix were added to the kaolin suspension.

Figure 26 shows the effect of adding drops of iodine solution to kaolin aqueous suspensions. Iodine has a very strong effect on the stabilization of kaolin suspensions. As observed, 1 drop of iodine solution helps stabilizing the suspension even after 24 h. In this test tube (I_1), a small and not fully transparent supernatant was visible only after 24 h of resting. On the other hand, when increasing the amount of iodine it was clear that the ideal amount of iodine had been exceeded. In Figure 26 a) it is visible that sediment starts to form immediately on the test tubes to which 3 and 4 drops of iodine were added. After 10 min of the addition of iodine (Figure 26 b)), these tubes had already big kaolin sediments at the bottom and the supernatant had started to show some transparency. On the test tube to which 2 drops of iodine solution was added, after 10 min, it was already possible to observe some kaolin sediment. After 24 h (Figure 26 c)), the sediments became more compact and the supernatants more transparent. As referred on the first chapter, this behaviour can be explained by the presence of an excess of free positive charge that ultimately results in lower ZP modulus values and decrease of the suspension stability when the ideal amount of iodine is exceeded [5].

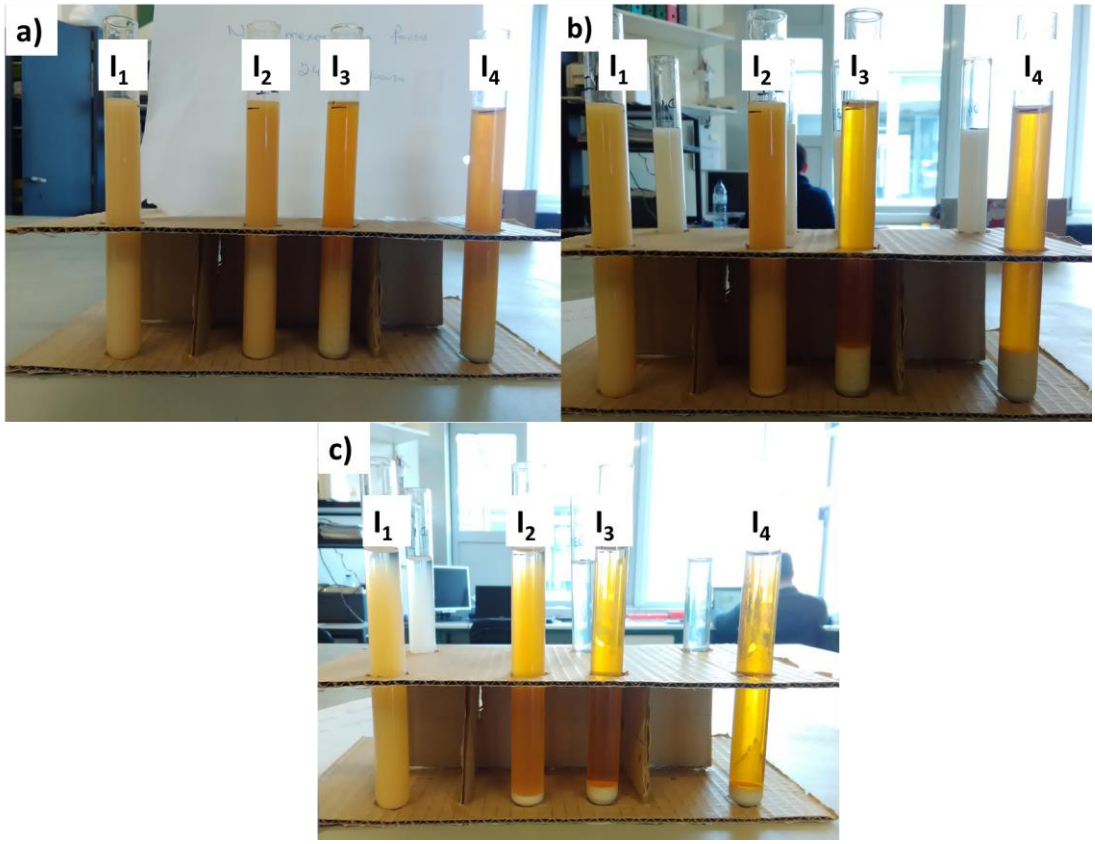

Figure 26 – Effect of the addition of iodine to kaolin aqueous suspension: a) immediately after the addition of 1, 2, 3 and 4 drops; b) after 10 min of resting and c) after 24 h of resting. The label I_n means that "n" drops of iodine were added to the kaolin suspension.

The evaluation of these results is made on a qualitative point of view in order to determine whether the additives influence or not the stability of kaolin suspensions. The concentration of additive per weight of solids was not precisely determined in the previous experiments. The variation of ZP *vs* amount of additive per weight of kaolin was assessed so that a more quantitative analysis of the influence of the additives was obtained.

Figure 27 shows the ZP variation of aqueous suspensions of kaolin with the amount (% of additive per weight of kaolin) of the additives Na_2SiO_3, Dolapix and I_2.

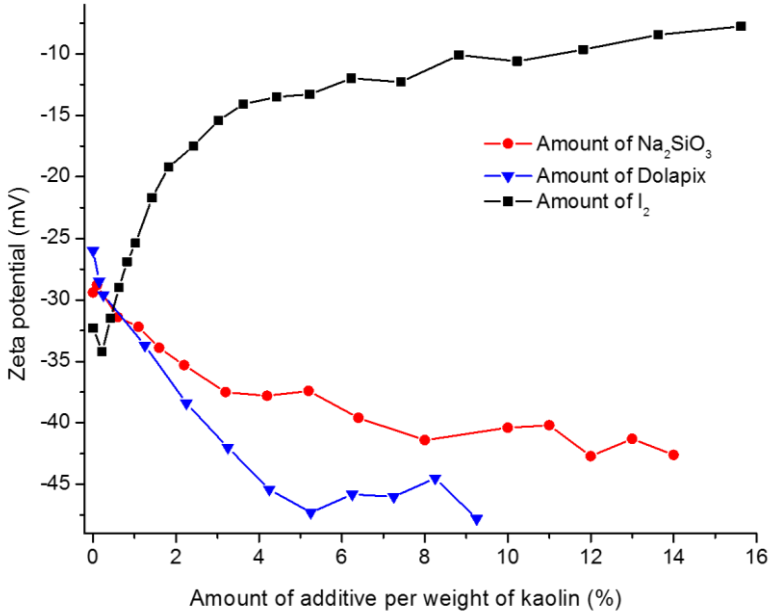

Figure 27 – ZP variation of kaolin aqueous suspensions as a function of the amount of Na_2SiO_3, Dolapix and I_2 by weight of kaolin.

ZP modulus tends to increase as the amount of Na_2SiO_3 and Dolapix increases. In the case of Na_2SiO_3, after the addition of 8 % the ZP does not evidence a significant change. In the case of Dolapix, the strong variation of ZP occurs until the addition of 5.3 %. The maximum values (in modulus) of ZP corresponding to these percentages are: -41.4 and -47.3 mV, respectively. In the case of I_2 there was a slightly increase of the ZP modulus at the beginning of its addition until - 34.2 mV and, after that the ZP modulus starts to decrease. This behaviour clearly evidences that an ideal amount of I_2 for maximizing the ZP exists and should not be exceeded to avoid decreasing the suspension stability. For this additive, the best ZP result (-34.2 mV) corresponds to the addition of 0.2 % of I_2.

Combining the additive concentrations highlighted by Figure 27 as the best ones to maximize ZP with aqueous suspensions of 10 g/l of kaolin, some EPD were performed in aqueous suspensions using the time and voltage conditions presented in Table 11. It was observed that deposition of kaolin could not be achieved for any of these trials. Voltages higher than 20 V were not tested because for high applied voltages water tends to suffer electrolysis which compromises the quality of the films.

Table 11 – Experimental conditions of voltage and deposition time used on the trials of EPD with aqueous suspensions using Na_2SiO_3, Dolapix and I_2 as additives.

Applied voltage (V)	5				10			15			20		
Time (min)	10	20	30	45	10	20	45	10	20	45	10	20	45

The ZP behaviours of ethanolic suspensions using I_2 as additive were also determined. In Figure 28, it is possible to compare the effect of adding I_2 to aqueous and ethanolic suspensions of kaolin.

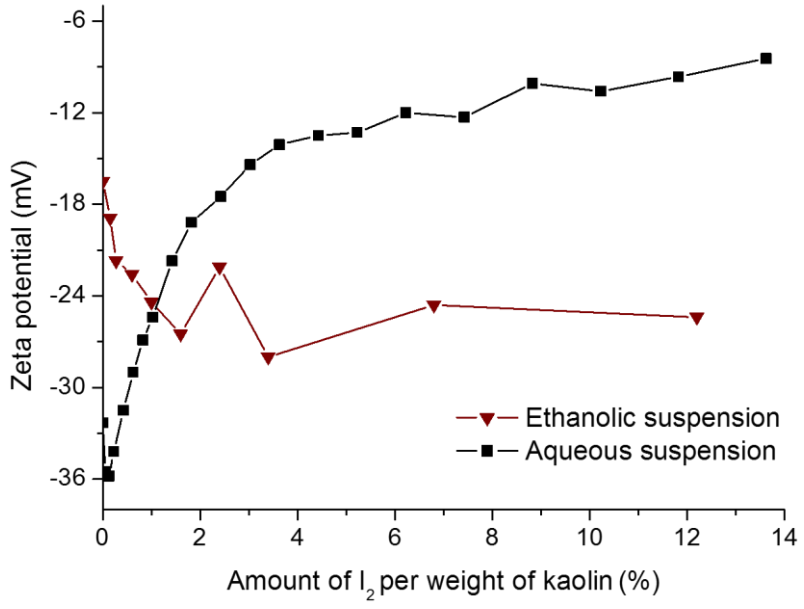

Figure 28 – Variation of ZP of aqueous and ethanolic suspensions of kaolin as a function of the amount of I_2 by weight of kaolin.

In Figure 28 it is observed that when adding I_2 to ethanolic kaolin suspensions the ZP values in modulus are higher than when I_2 is added to aqueous suspensions, after the addition of around

1 wt. % of I_2. This is an indicator of better particle charging effect and better stability for ethanolic suspensions. In Figure 29, it is possible to observe with more detail the iodine effect only for low concentrations of I_2 on ethanolic suspensions. The yellow ellipse identifies the interval of I_2 concentration to which corresponds the higher values of ZP modulus and hence to a stable suspension behaviour. Therefore, the selected concentration of I_2 to perform EPD using ethanol as suspension media was 1 % of I_2 per weight of kaolin.

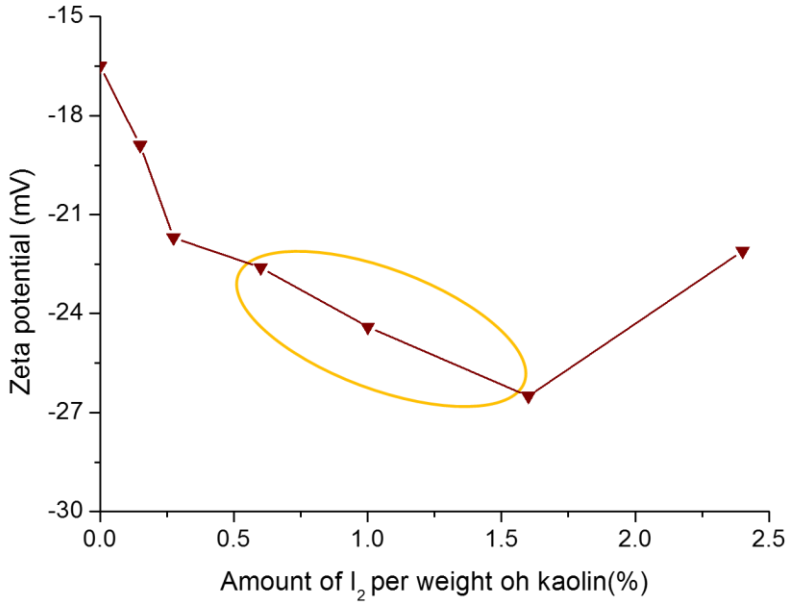

Figure 29 – Effect of the addition of I_2 to kaolin ethanolic suspensions highlighting the region of better ZP results.

Since aqueous depositions were not successful, it was decided to perform EPD using ethanol as suspension media and I_2 as additive. The combination of ethanol with I_2 as additive is frequently referred on literature about EPD as described on the first chapter (see Table 2). The selected voltage was 20 V because initially the idea was to increase the water content of the suspension media so that it could be more "eco-friendly" and less expensive (high voltages lead to electrolysis). Several attempts were carried out with aqueous, mixtures of ethanol and water and ethanolic suspensions. The results showed that the best conditions for EPD of kaolin were those combining ethanol and water in a (water: ethanol) molar portion of (1:9). The first successful depositions were run in ethanol with iodine at 20 V for 10, 15 and 20 min. After this, depositions, in which the suspension media was a solution of ethanol and water in a (water: ethanol) molar portion of (1:9), were performed. When higher molar fractions of water were tested, no depositions occurred. Later, when trying to obtain a second batch of films using only ethanol as suspension

media, no deposition occurred as well. This phenomenon lead to the conclusion that a small amount of water is necessary to obtain kaolin films by EPD. The first deposition only occurred because the ethanol was aged and already had some water on its constitution. When new ethanol was used, no deposition occurred.

Regarding the deposition times, 15 min was chosen as the ideal time to perform deposition at 20 V. For shorter times, the obtained films were not uniform since parts of the substrate remained uncovered being still visible after deposition. For longer deposition times, it was possible to observe that the thickness of the film was irregular. The films presented thickness gradients, being thicker at the bottom, which meant that after 15 min of deposition, sedimentation was prevailing over deposition.

In order to better understand the effect of I_2 on kaolin suspensions, UV transmittance of these suspensions was measured during 15 min. The results can be observed in Figures 30, 31 and 32. The transmittance variation (ΔT) of each suspension expressed as the difference between the final and initial values of transmittance is given in Table 12. Ideally, for EPD processes, transmittance should be low and constant over time which means that the particles remain well dispersed and in suspension [5].

Table 12 – Transmittance variation of kaolin suspensions with and without I_2.

Suspension media	$T_{initial}$ (%)	T_{final} (%)	ΔT (%)
Water	47.5	56.6	9.1
Water + I_2	44.1	53.5	9.4
Ethanol	58.7	70.4	11.7
Ethanol + I_2	51.6	65.3	13.7
Ethanol + water	52.2	65.1	12.9
Ethanol + water + I_2	53.7	65.9	12.2

In Figure 30, it is visible that for both aqueous suspensions there is an increase of transmittance over time which means that sedimentation of the particles occurs. The increase of the transmittance is around 9 % after 15 min for both suspensions. Therefore, neither one of the suspensions can be considered as fully stable. The transmittance of the suspension with I_2 is always around 3 % lower than the suspension without I_2. This shows that iodine helps stabilizing the particles in suspension. The same effect is visible in Figures 24 and 26: when comparing test tube

S_0 with test tube I_1 after 24h it was visible that the kaolin sediment was smaller on the test tube to which I_2 was added.

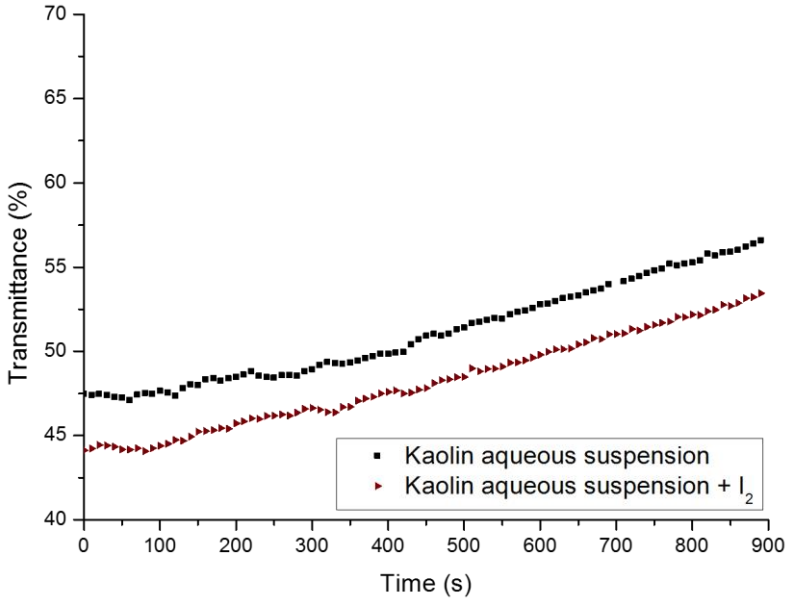

Figure 30 – UV light transmittance (%) *vs* time for kaolin aqueous suspensions with and without I_2.

In Figure 31, it is observed that the ethanolic suspension with I_2 presents a transmittance which is around 6 % lower over time than the suspension without I_2. Therefore, I_2 also has a positive effect on the stability of ethanolic suspensions of kaolin. There is a variation of transmittance over time in both cases although the suspension with I_2 shows a larger variation of transmittance over time. Once again, these suspensions are not fully stable because the transmittance is not constant over time.

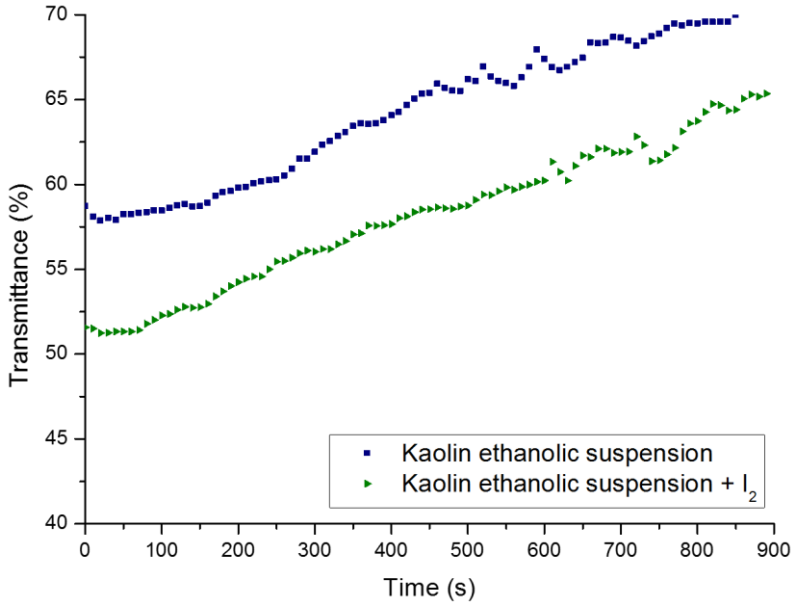

Figure 31 - UV light transmittance (%) *vs* time for kaolin ethanolic suspensions with and without I_2.

When comparing Figures 30 and 31, it is possible to see that aqueous suspensions show better results of stability which may indicate them as better suited for EPD. On the other hand, when observing Figure 28, the better ZP results are observed for the ethanolic suspensions. The worst ZP results for aqueous suspensions and the fact that water tends to suffer electrolysis explains why EPD with aqueous suspensions of kaolin does not result.

Figure 32 shows that both ethanolic suspensions, to which some water was added to the ethanol, with and without I_2 present a quite similar transmittance behaviour, being the difference between the initial and final values of transmittance of the suspensions around 1 %. Both transmittance values are not constant, showing an increase of around 12 % in both cases which implies sedimentation over time. In this case, I_2 does not seem to have a significative influence on the stability of the particles as it did on the other suspension media.

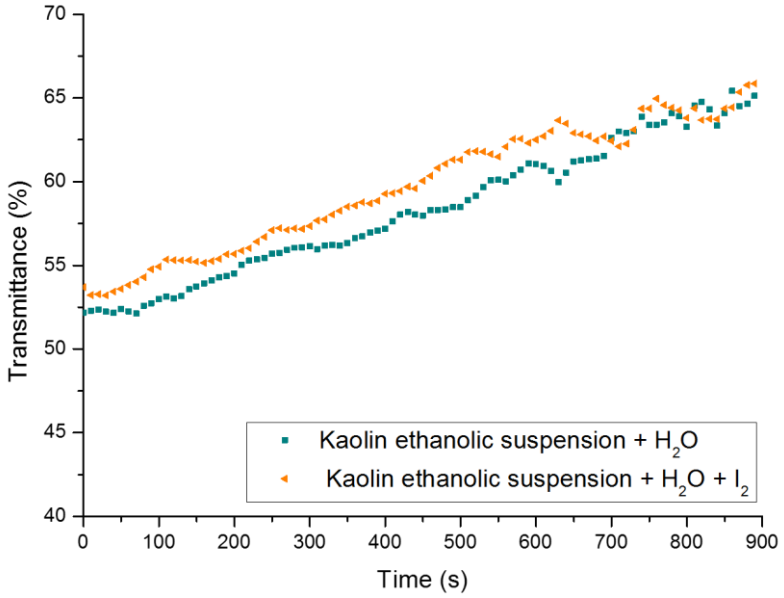

Figure 32 - UV light transmittance (%) *vs* time for kaolin suspensions of $\chi_{mol.water}$ = 0.1 and $\chi_{mol.ethanol}$= 0.9 with and without I_2.

EPD only resulted when water and I_2 were added to the ethanolic suspension media although these conditions do not present the best results in terms of transmittance. The transmittance of a suspension is not enough to fully understand the effect of the presence of a small fraction of water and I_2 to the suspension media. In Figure 33 is presented a comparison between the behaviours of all the suspensions where ethanol is used as the main component of the suspension media.

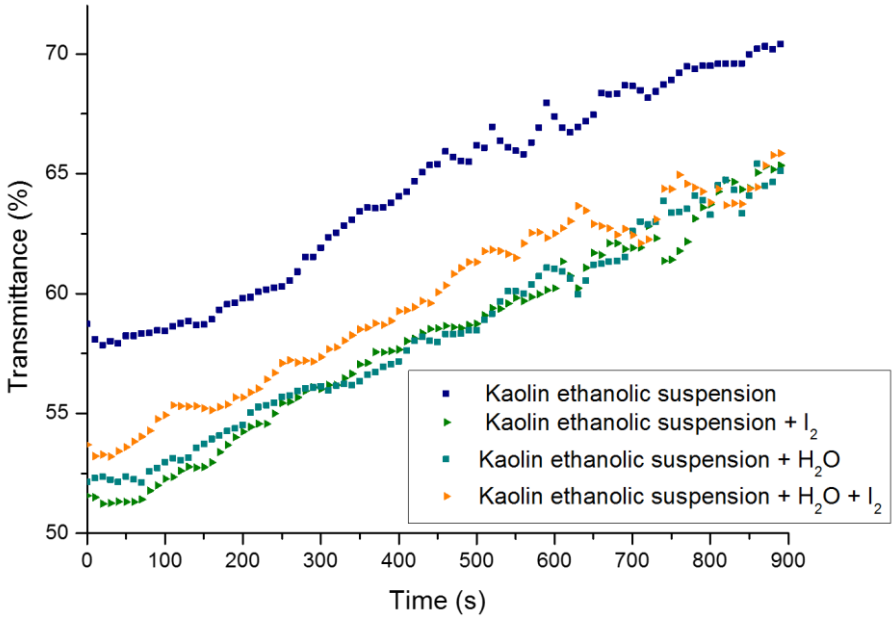

Figure 33 – Comparison of the UV light transmittance variation (%) over time for the different media prepared with ethanol.

The comparison of the curves respecting the two suspensions without I_2 shows that the addition of water to the suspension media decreases de transmittance around 6 % over time relatively to the suspension without water. The effect of water with I_2 cannot be fully understood only by interpretation of the transmittance results. Apart from the ethanolic suspension, the other three suspensions show a similar behaviour. Even not representing the best transmittance results, the only suspension that allows kaolin films to be produced by EPD is the one of which the suspension media is composed of ethanol (χ_{mol} = 0.9), water (χ_{mol} = 0.1) and I_2 (1 wt. % of the wt. of kaolin).

To measure ZP, one of the required parameters to define on the equipment is the suspension media. The available options on the equipment are only for single liquids and not for mixtures. Since the fraction of water is small, an attempt to measure ZP *vs* amount of I_2 of the suspension with ethanol and water was made considering ethanol as suspension media. The results are presented in Figure 34 that shows, for comparison purposes, the dependence of the ZP with the added amount of I_2 of both the ethanolic suspension and the ethanol with water suspension.

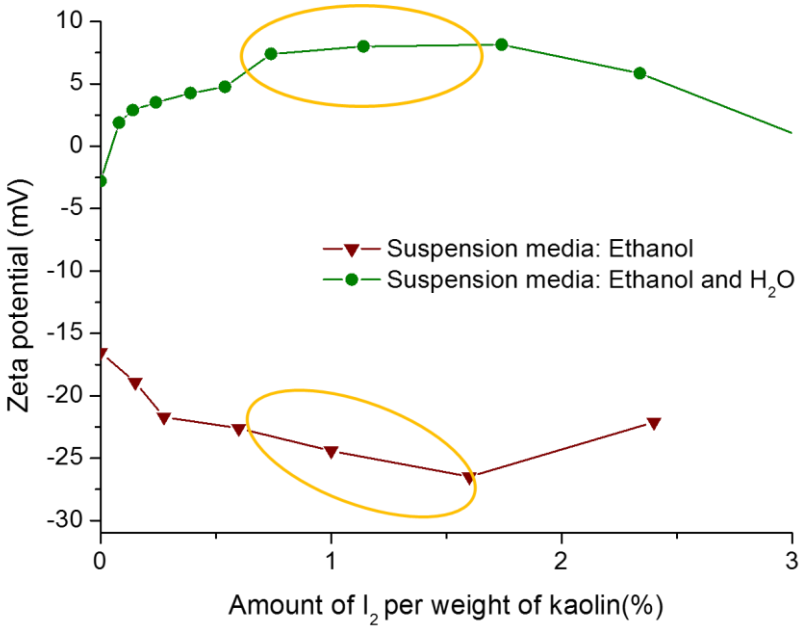

Figure 34 - Variation of the ZP of kaolin suspensions with the added amount of I_2 (per weight of kaolin) for two different suspension media: ethanol (χ_{mol} = 1) and etanol (χ_{mol} = 0.9) + water (χ_{mol} = 0.1).

When no I_2 is added to the suspension, the ZP values of both suspensions are significantly different and that difference tends to increase with the addition of I_2 which is probably an indicator that even a small amount of added water that is not given as a parameter to the equipment is enough to influence the data. The main conclusion to be taken from Figure 34 is that, even though the ZP values are probably shifted from the real ones, the region of I_2 concentration for which the ZP is stable and has higher modulus is the same for both suspensions (highlighted with yellow ellipses). After this region, the ZP modulus starts to decrease which also means that an ideal amount of I_2 cannot be exceeded for this kind of suspension. As said before, according to the UV light transmittance results, the addition of water to the suspension media without any I_2 improves the stability of kaolin suspensions relatively to the ethanolic suspension (Figure 33). In Figure 34 it is visible that the addition of around 1 wt. % of I_2 to both suspensions leads to higher ZP modulus than when no I_2 is added. Even though the process is not yet fully understood and explained, the combined effect of added water and I_2 seems to be a key parameter to successfully obtain kaolin films by EPD.

The behaviour of the ethanol suspensions (with 1 % wt. of I_2) either without water or added with an amount of water exceeding χ_{mol} = 0.1 is described in Figure 35. In both cases, the suspension loses stability right after connecting the electrical source and a big kaolin sediment forms in a few seconds.

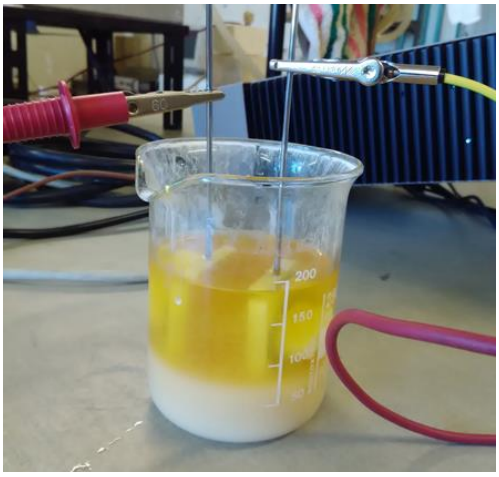

Figure 35 – Kaolin sediment formation on suspensions with no added water or with more than χ_{mol} = 0.1 of added water.

Koura *et al.* [17] proposed a mechanism for the formation of protons in which the addition of I_2 and H_2O to the suspension media was necessary (Equations 3 and 4). In Koura *et al.* [17] work, the suspension media is acetone and therefore the mechanism cannot be applied to this work. Nevertheless, the effect of iodine is often explained by the generation of protons that are adsorbed on the surface of the suspended particles (for ethanol and for acetone as suspension media) [5] [15] [17]. The adsorption of protons makes the particles positively charged which leads to deposition at the negative electrode. In this work, the films were obtained at the negative electrode. Therefore, it is very likely that the I_2 and water addition effect can be explained by a mechanism similar to the one proposed by Koura *et al.* [17] but for ethanol as suspension media.

3.3 Kaolin thick films and bulks

Using the above referred EPD conditions, kaolin films were prepared. Three kinds of substrates were used: stainless steel, platinum foil and platinized silicon. Apart from the substrate type, all the deposition and sintering conditions were the same.

Stainless steel substrates allowed good quality kaolin green films (KGr) films to be obtained but they were damaged after sintering. The substrates could not withstand the high sintering temperatures. The oxidation of the substrate lead to the destruction of the films as presented in Figure 36. After sintering at 1200 ^{o}C for 2 h, the films were cracked and separated from the substrate.

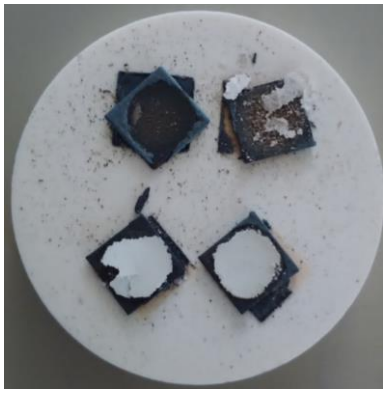

Figure 36 – Sintered kaolin films (KF) on stainless steel substrates after sintering at 1200 °C for 2 h.

To avoid problems while sintering, platinum foil substrates were used. These substrates are too thin to be used on EPD cells and became easily wrinkled when handled. Lots of bumps are formed when the substrate is placed on the electrophoretic cell which prevents the films to be flat. To perform hardness tests, the films surface needs to be flat and their thickness must be well determined because the indenter cannot reach the substrate. Such irregularities on the films surfaces did not allow proper thickness measurements thus compromising subsequent nanoindentation tests.

To test the mechanical properties, a last batch of films was deposited on platinized silicon substrates. These substrates resist to the sintering temperatures and are more rigid and thicker than the platinum foil substrates which allows accurate thickness measurements. After sintering, the films were flat and the adhesion to the substrate was not compromised as presented in Figure 37. Both the films sintered at 1200 and 1300 °C show regular surfaces and well defined edges. The irregularities on the KF_{1200} edge, visible in Figure 37 a), were caused when the film was removed from the electrophoretic cell.

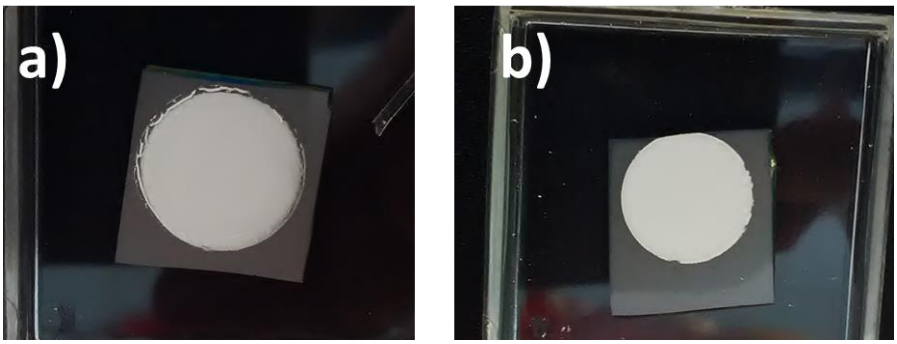

Figure 37 – KF on platinized silicon substrates: a) sintered at 1200 °C, for 2 h and b) sintered at 1300 °C, for 2 h.

3.3.1 Kaolin green films (KGr)

For all the KGr, the initial and final electrical currents of deposition were recorded. The KGr were also weighed. These results are presented in Table 13.

Table 13 – Average weight, initial and final deposition current of KGr for each kind of used substrate.

	Substrate type		
	Stainless steel	**Platinum foil**	**Platinized silicon**
Average deposited mass (mg)	4.7	5.0	5.1
Average initial current (mA)	0.23	0.39	0.47
Average final current (mA)	0.17	0.23	0.24

The deposited mass is always around 5 mg which implies that the amount of deposited material is independent from the kind of substrate. For all the substrates, there is a decrease of the current during deposition. This is due to the fact that while the film is forming, the formation of an insulating layer of ceramic particles on the electrode is occurring.

KGr top view were observed using an optical magnifier. In Figure 38, it is possible to compare the KGr deposited on platinum foil (Figure 38 a)) with the KGr deposited on platinized silicon (Figure 38 b)). KGr on platinum foil shows a much less flat surface and its edges are not well defined and are rougher than those of KGr on platinized silicon substrates. The higher thickness and rigidness of the platinized silicon substrates allows better quality green films to be obtained.

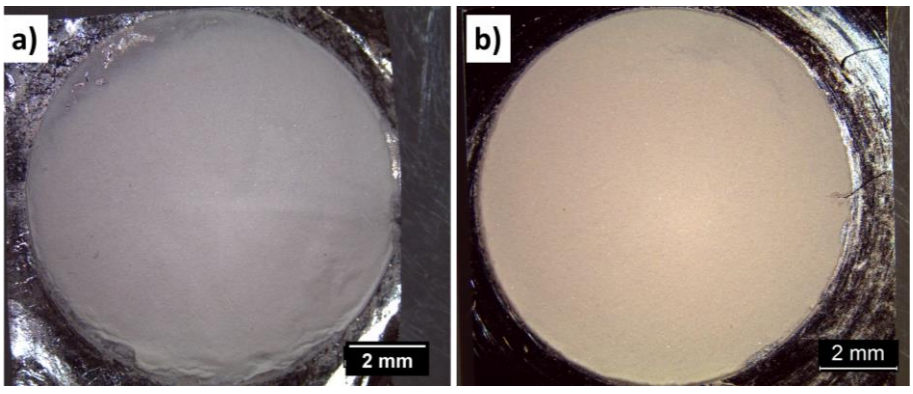

Figure 38 – Optical magnifier images of: a) KGr deposited on platinum foil and b) KGr deposited on platinized silicon.

SEM micrographs of the KGr are presented in Figure 39. In Figure 39 a) some cracks are visible on the film surface. These cracks were probably formed during the drying step due to the stress induced by non-uniform retraction. Regarding the particles orientation, it is possible to observe in Figure 39 b) that there is a tendency for the basal surfaces of kaolin particles to be aligned parallel to the substrate surface. Layers of stacked kaolin lamellar particles are visible on some parts of the micrograph. It is also visible that the film is highly porous.

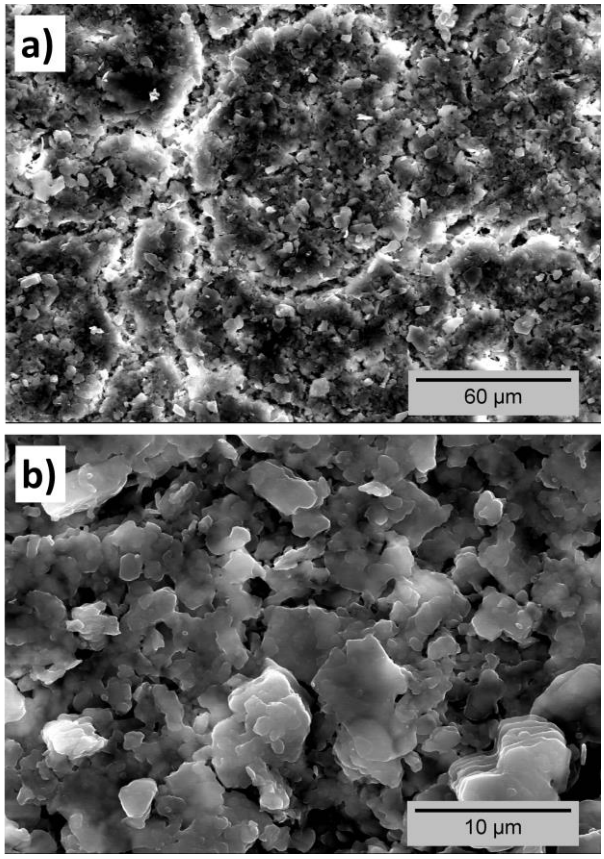

Figure 39 – SEM micrographs of KGr: a) showing a top view of the surface and b) a magnified detail of the microstructural organization.

3.3.2 Sintered films (KF) *vs* sintered bulks (KB): structure and microstructure

Kaolin films and pellets were sintered at 1200 and 1300 ^{o}C, for 2 h with heating rates of 10 ^{o}C/min. The XRD patterns of KF an KB samples can be observed in Figures 40 and 41, respectively. To complement the XRD analyses, RIR method was used to quantify the phases. In the case of the films, the XRD patterns were obtained considering platinum not as a distinct layer but as a homogeneously distributed phase which introduces some errors on the phase quantification. A way to avoid these errors would have been to obtain XRD patterns using the grazing angle XRD

technique which requires completely flat and regular film surfaces which was not the case even for the KF deposited on platinized silicon substrates. The films always present some small irregularities on the edges and surfaces which does not allow the use of the technique.

The XRD patterns represented in Figure 40 show that KF are constituted of mullite and cristobalite which are, according to Chakraborty *et al*. [24], the expected phases after sintering kaolin. The presence of the platinum peaks is due to the substrate. It is visible that the platinum peaks intensity is higher for KF_{1300} than for KF_{1200} which is an indicator that KF_{1200} are thicker than KF_{1300}. Using RIR method, a quantification of the phases was calculated. In Table 14, it is possible to see that KF_{1300} have more than 10 % of mullite on its constitution than KF_{1200} which shows that higher sintering temperatures enhance mullite formation. It is important to consider that these percentages may not correspond to the real phase amounts, as previously explained, due to the presence of the substrate, these phase quantities allow the comparison between KF_{1200} and KF_{1300} in terms of quantity of formed mullite although they should not be compared with the phase quantification presented for KB in Table 15.

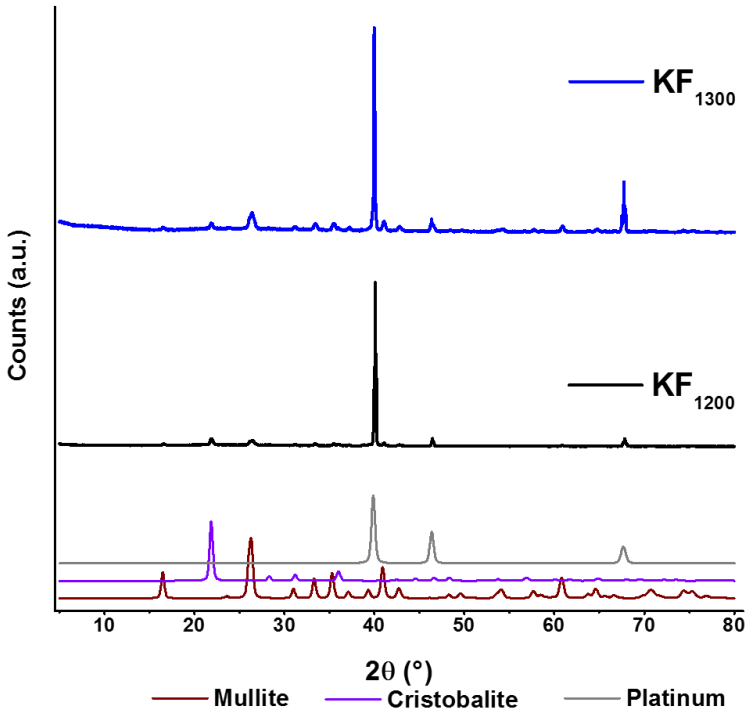

Figure 40 – XRD patterns of kaolin films sintered for 2 h at 1200 °C (KF_{1200}) and at 1300 °C (KF_{1300}).

Table 14 – KF phase quantification calculated using RIR method.

	KF_{1200}	KF_{1300}
Mullite (%)	81.7	94.4
Cristobalite (%)	18.3	5.6

The XRD patterns represented in Figure 41 show that KB have not only mullite and cristobalite on their constitution but also quartz. For around 2θ=10 °, a hump is visible in both XRD patterns which indicates that some amorphous or not crystallized phase is probably present. Since the hump is less evident for the KB_{1300}, it is probably because that phase tends to crystallize with the increase of temperature. KB phases were also quantified using RIR method. The results are presented in Table 15 where it is possible to see that higher temperatures also enhance mullite formation on KB.

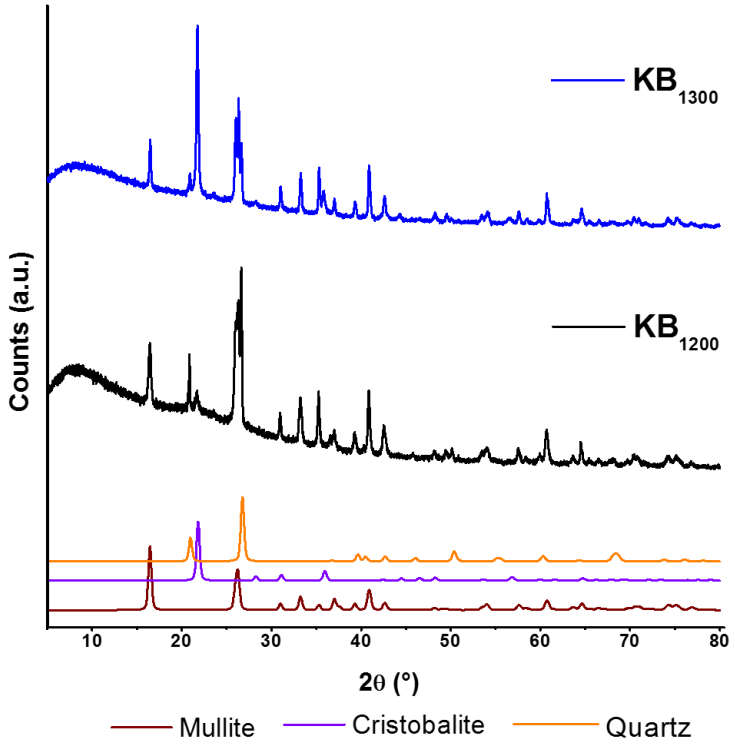

Figure 41 - XRD patterns of kaolin bulk samples sintered for 2 h at 1200 °C (KF_{1200}) and at 1300 °C (KF_{1300}).

Table 15 - KB phase quantification calculated using RIR method.

	KB_{1200}	KB_{1300}
Mullite (%)	71.9	80.7
Cristobalite (%)	1.9	4.6
Quartz (%)	26.9	14.7

KF and KB have a different phase constitution as quartz is only present on KB ant it was not detected on KF. This may be a result of the influence of the substrate since it induces tensions on the ceramic film that may interfere on the phase formation. The different conditions to which the material is exposed when deposited and sintered on top of a substrate are probably favourable to the transformation of quartz (that exists in the used kaolin powders) into cristobalite.

KF and KB microstructures were observed by SEM. A comparison between KF_{1200} and KF_{1300} microstructures will be established with regard to their counterpart KB.

Figure 42 shows top view and cross sections of KF_{1200} deposited on platinum substrates. The micrograph in Figure 42 c) was obtained from a cracked piece of film that was sintered on a stainless steel substrate that ended up loose after sintering. As observed in the SEM micrographs of KGr, Figure 42 a) shows that KF_{1200} also has cracks on the surface. When comparing the top view with the cross section micrographs, it is possible to observe that the basal planes of kaolin particles tend to be aligned parallel to the substrate. Despite this tendency, in Figure 42 b) and d), it is possible to observe that not all the particles are completely oriented and that some porosity is still present. Figure 42 e) shows a cross section of the film deposited on the platinum foil substrate. This film shows high thickness irregularities and it is visible that the substrate is bended.

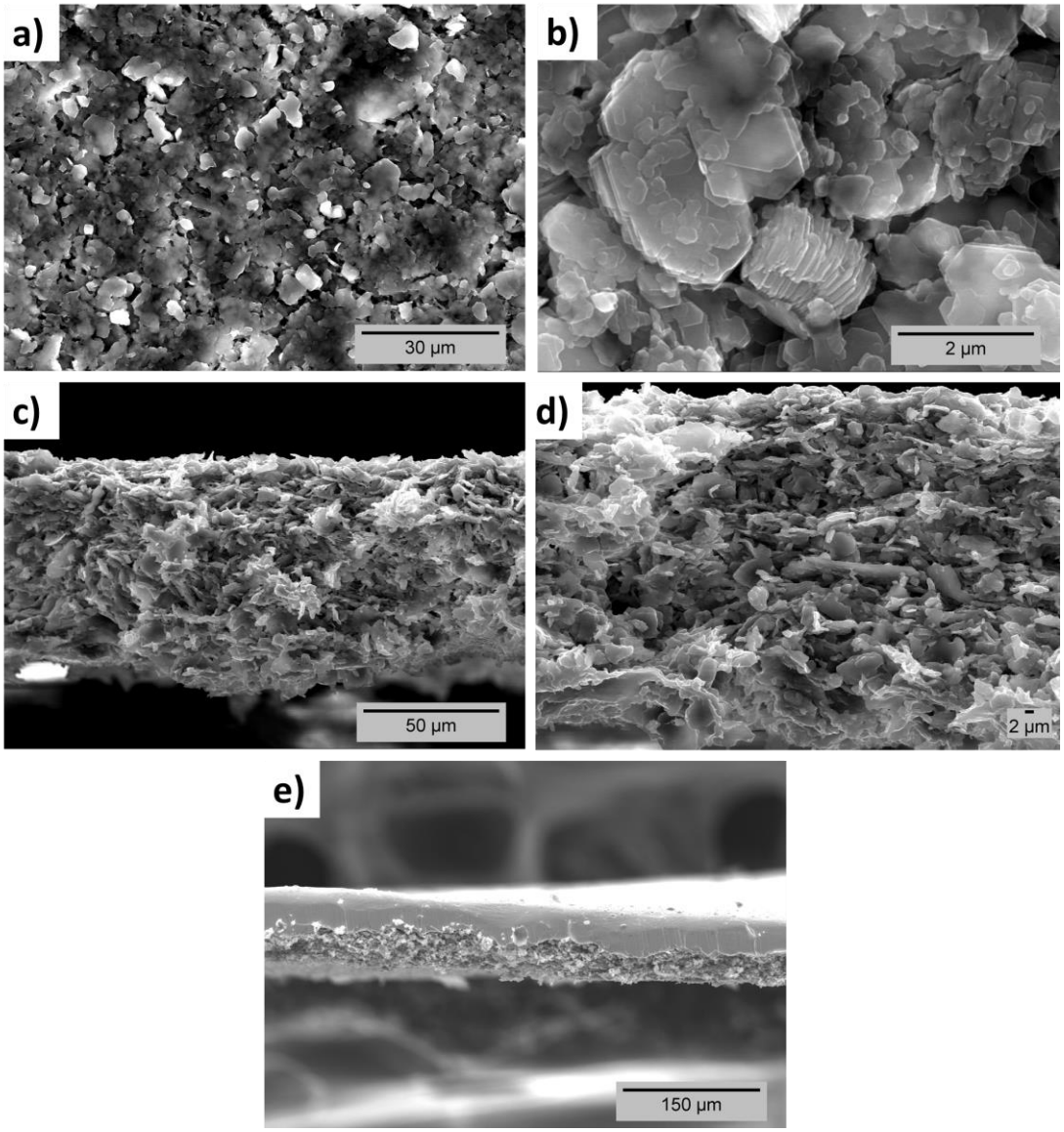

Figure 42 – SEM micrographs of: a) and b) KF_{1200} top view and with different magnifications and c), d) and e) KF_{1200} cross section with different magnifications.

Figure 43 shows the microstructure of KF_{1300} deposited on platinum substrates. These films are similar to the KF_{1200} is terms surface quality and of particle orientation. In Figure 43 a) and b) it is visible that the particles tend to be aligned with the basal planes parallel to the substrate. Some cracks on the surface are visible in Figure 43 a). Figure 43 c) shows many thickness irregularities due to the platinum substrate being bended.

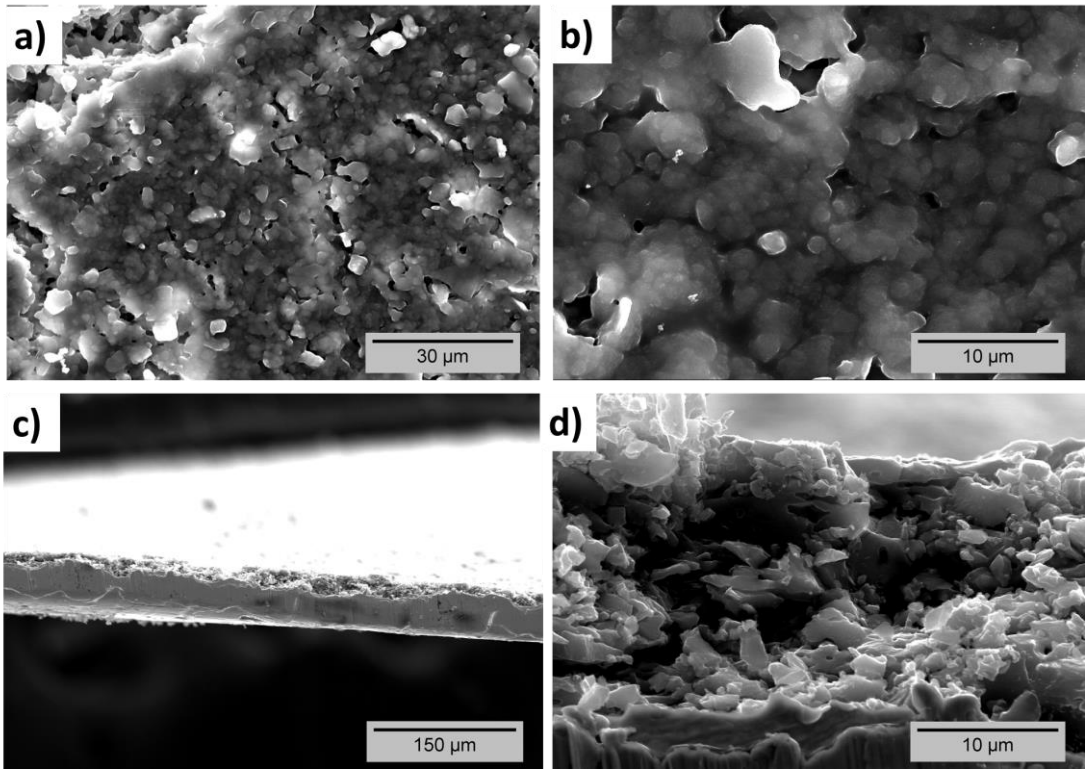

Figure 43 – SEM micrographs of: a) and b) KF_{1300} top view and with different magnifications and c) and d) KF_{1300} cross section with different magnifications.

When comparing Figure 42 b) and d) with Figure 43 b) and d) it is visible that KF_{1300} present a more densified microstructure than KF_{1200}. Whereas KF_{1200} still present particles with well-defined shape and pores between them, KF_{1300} do not present particles with such well-defined shape and less porosity is evidenced on the micrographs. In Table 16, are presented the thickness values estimated by ImageJ for the KF_{1200} and the KF_{1300} deposited on platinum foil.

Table 16 – Thickness estimation by ImageJ of KF_{1200} and KF_{1300} deposited on platinum foil obtained using ImageJ.

	KF_{1200} on platinum foil	**KF_{1300} on platinum foil**
Average thickness (µm)	34.3	14.3
Minimum thickness (µm)	24.8	4.4
Maximum thickness (µm)	42.0	23.4
Standard deviation	5.3	5.3

The estimated thicknesses for KF_{1200} are higher than the estimated thickness for the KF_{1300} which shows, like the micrographs, that KF_{1300} is denser than KF_{1200}. For both KF_{1200} and KF_{1300} sintered on platinum substrates, the results in Table 16 show that this kind of substrate leads to the production of very irregular films. Big differences between the minimum and maximum thickness of the films were observed which clearly shows the negative effect of the platinum foil substrates on the regularity of the films.

Progressively, better quality could be obtained as the type of substrate was changed. A comparison between the KF deposited on platinum foils an KF deposited on platinized silicon substrates can be established based in Figure 44 and Figure 45. In both cases, using platinized silicon substrates leads to less rough films with more well defined edges.

KF_{1200} present better quality surface than KF_{1300} when sintered on platinum foil substrates. In this case, KF_{1300} had visible cracks spread all over the surface. The roughness of the substrate induced stresses and non-uniform shrinkage on the film while sintering which lead to crack formation. At 1200 ^{o}C, shrinkage is not so intense and therefore no cracks are visible in the amplified images. When platinized silicon substrates were used, no visible cracks were observed for any of the temperatures.

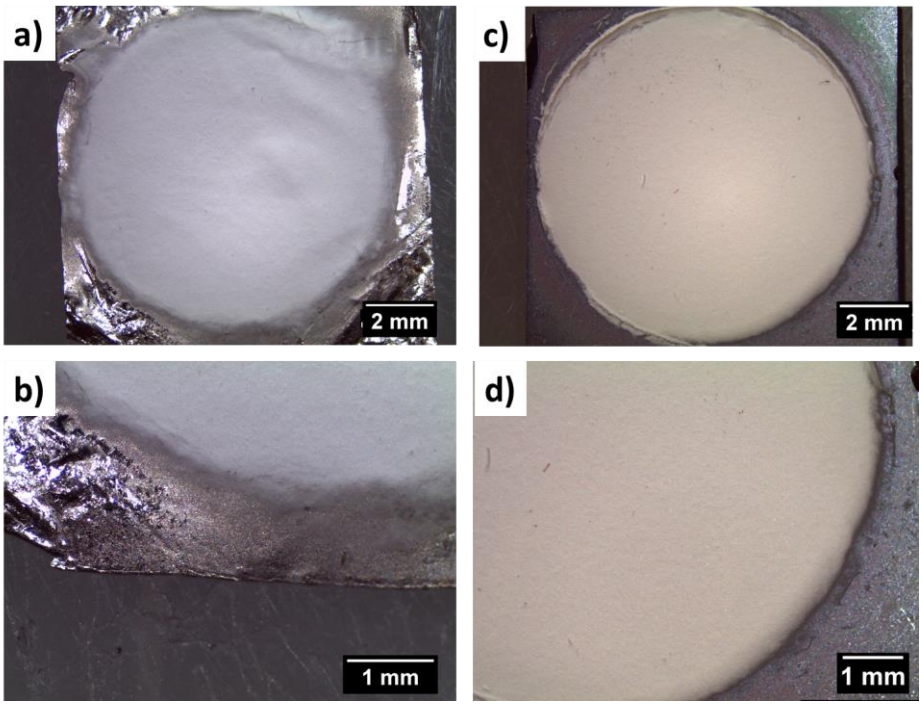

Figure 44 - Optical magnifier images of KF_{1200}: a) and b) film on platinum foil substrate; c) and d) film on platinized silicon substrate.

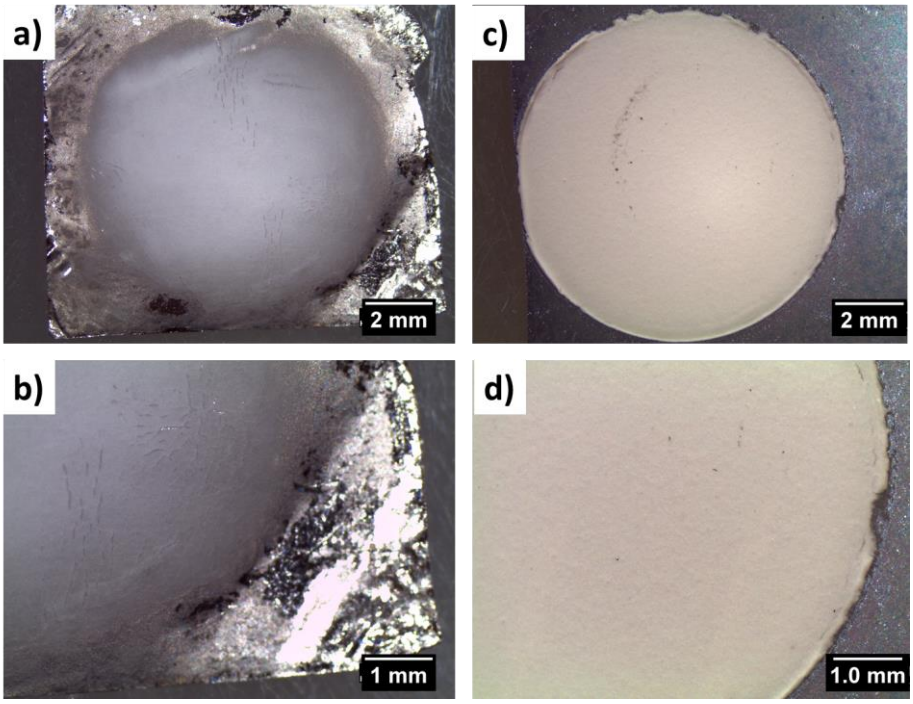

Figure 45 - Optical magnifier images of KF_{1300}: a) and b) film on platinum foil substrate; c) and d) film on platinized silicon substrate.

Since films with more regular surfaces and thicknesses were deposited on platinized silicon substrates it was possible to measure their thicknesses using a micrometer. Average thicknesses of KF_{1200} and KF_{1300} are presented in Table 17. These values result from the thickness difference between the substrate and the total thickness of the substrate plus the film. Measurements were made on the film center considering that this part is more regular than the edges. KF_{1200} are thicker than KF_{1300} which is due to higher shrinkage and densification when the material is sintered at 1300 ^{o}C. As compared to the values presented in Table 17 the thickness values presented in Table 16 are viewed as an estimation since they were obtained from micrographs which may not be representative of the whole sample.

Table 17 –Average thickness of KF_{1200} and KF_{1300} deposited on platinized silicon substrates.

Film	Average thickness (µm)
KF_{1200}	47
KF_{1300}	41

In Figures 46 and 47, is it possible to observe KB microstructures. Top view and cross sections of both KB_{1200} and KB_{1300} were observed. Regarding the cross sections, both polished and fracture surfaces were observed. To obtain these SEM micrographs it was necessary to submit the material to chemical etching that was done using fluoridric acid but it was not completely effective and the grain boundaries are not well visible especially for KB_{1300}.

In Figure 46, it is visible that some porosity is still present on KB_{1200}. On the other hand, $KB1_{300}$ have a much more densified structure and the amount of visible porosity is lower, as can be observed in Figure 47. Since the quality of the chemical etching compromised the quality of the SEM micrographs and did not allow to observe the orientation of the particles, an observation of the fracture surfaces was made. Figure 46 c) and Figure 47 c) show once more that KB_{1300} are denser than KB_{1200}. On these micrographs, no preferential orientation of the particles could be claimed.

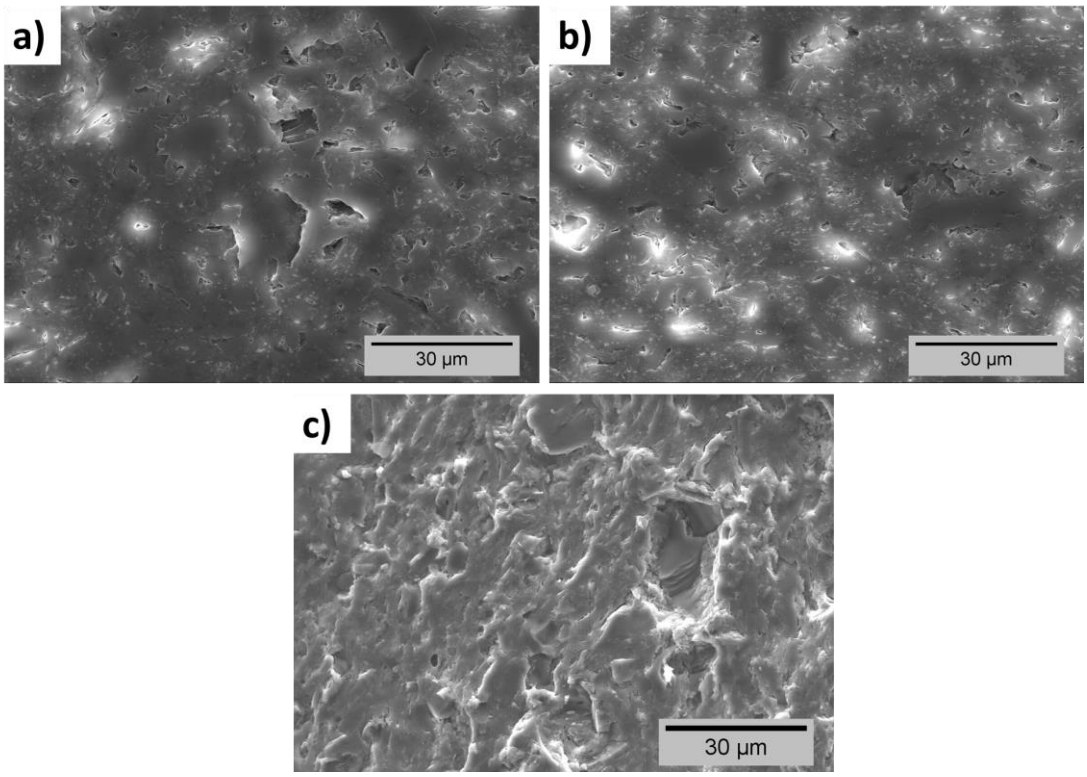

Figure 46 – KB_{1200} SEM micrographs: a) polished surface top view; b) polished surface cross section and c) fracture surface cross section.

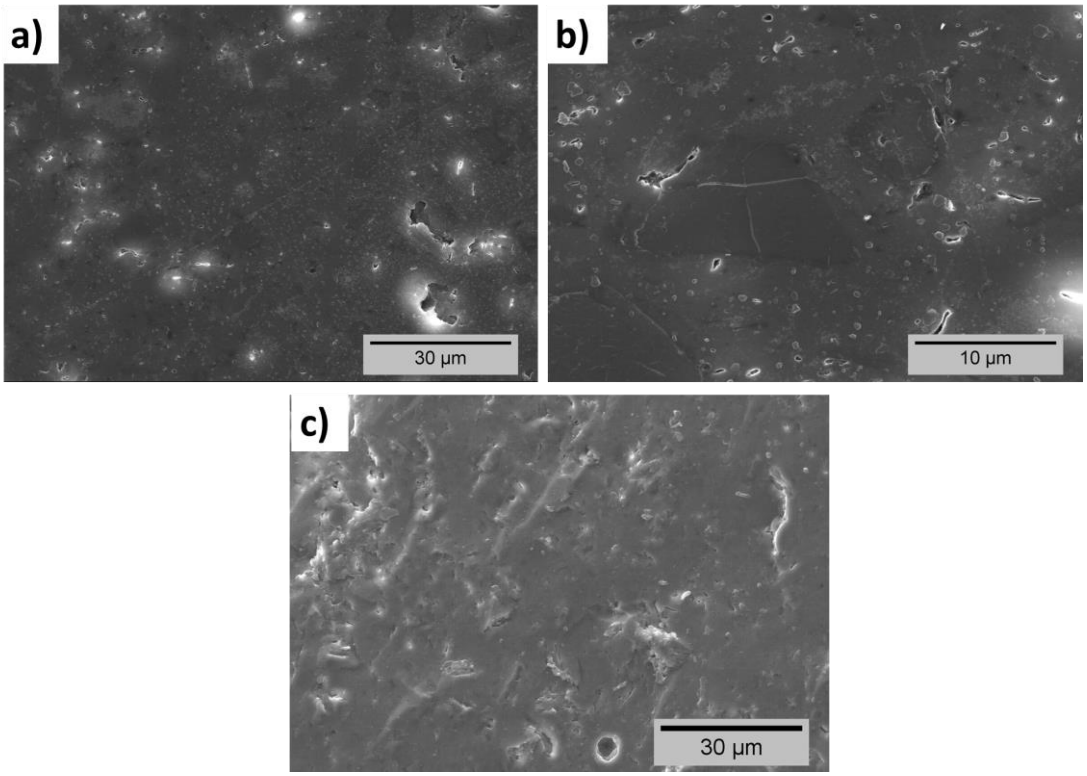

Figure 47 – KB_{1300} SEM micrographs: a) polished surface top view; b) polished surface cross section and c) fracture surface cross section.

From all the SEM micrographs, comparisons between KF and KB microstructures can be made in terms of densification and particle orientation. KB are always denser than KF which is expectable since the green density of green pressed bodies is higher than when green films are obtained by EPD. On the other hand, a preferential orientation is only visible on KF which was one of the objectives of this work. Processing kaolin by EPD lead to the production of films on which many of the particles have a preferential orientation.

3.3.3 Mechanical properties of KF and KB

Mechanical properties of KF and KB were assessed by nanoindentation tests under the same conditions. From these tests, some parameters were obtained based on force *vs* displacement curves which allowed the calculation of the average Vickers hardness and Young's modulus of the produced materials. It is very important to keep in mind that nanoindentation is a very local technique and thus the obtained results may reflect contributions due to heterogeneities of the material. When the indenter contacts with the material, it is not possible to ensure that the contact occurs in a region with the same characteristics for each of the indentations. In the case of a ceramic, the indenter may contact the center of the grains or the grain boundaries thus affecting

the mechanical properties response. Porosity is another factor contributing to different mechanical response. When the indenter contacts with a densified part of the material the mechanical response is different from that of a less densified part of the material. Taking these aspects into account, the average Vickers hardness (HV_{IT}) and the average Young's modulus (E_{IT}) of KF and KB are represented in Figures 48 and 49 with the respective error bars.

The Vickers hardness of KF is around 300 MPa whereas that of KB is around 1200 and 1950 MPa for the KB_{1200} and the KB_{1300}, respectively, being thus concluded that KB are harder than KF. This reflects the higher density of KB as observed on the previously presented SEM micrographs. From the SEM micrographs, it was observed that KF_{1300} (Figure 43) seemed denser than KF_{1200} (Figure 42) which suggest a higher hardness for KF_{1300} as compared to KF_{1200}. Although the results indicate a lower average Vickers hardness for KF_{1300} it is also observed that the uncertainty associated to the KF_{1300} results is larger as compared to that of KF_{1200}. This may indicate that the indentations were made on regions with different properties. A larger number of indentations on different films is here recommended in order to increase the significance of the results.

Regarding the statistical significance of the presented results, in addition to the fact that the indentations may reflect the heterogeneity of the materials, another fact may be taken into consideration as well. Ceramics are typically brittle which difficults the achievement of accurate hardness measurements. Due to the brittle behaviour, the ceramics are prone to crack when the indenters are forced into their surfaces [18].

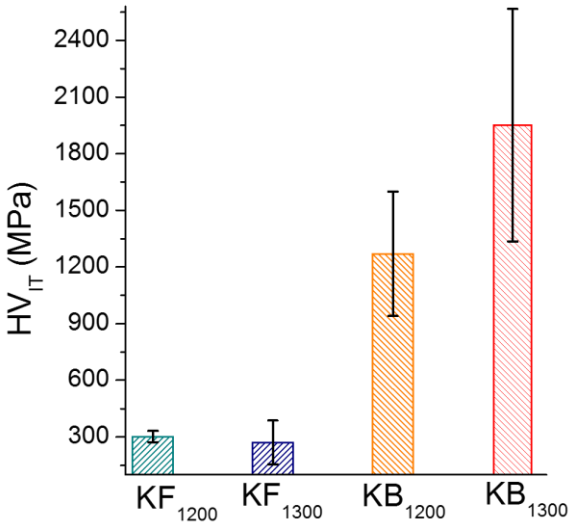

Figure 48 – KF and KB average Vickers hardness calculated from the force *vs* displacement curves obtained from the nanoindentation testes and respective error bars.

The Young's modulus of KF is around 40 GPa whereas that of KB is around 90 and 100 GPa for the KB_{1200} and the KB_{1300}, respectively. KB present higher Young's modulus than KF which is accordingly to the Vickers hardness results. The properties of ceramic materials result from the atoms they are constituted but also from the type of bond between them. On ceramics, strong ionic and covalent bonds are dominant. As a result, from these types of bonds, ceramics tend to present high Young's modulus and high hardness [46].

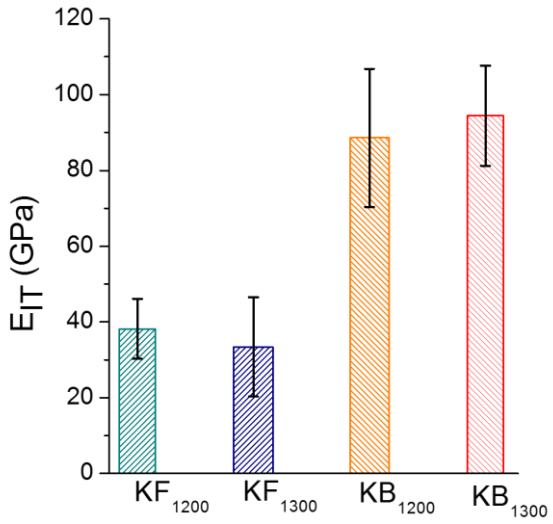

Figure 49 - KF and KB average Young's modulus calculated from the force *vs* displacement curves obtained from the nanoindentation testes and respective error bars.

Considering that mullite is the main constituent of KB after sintering, the obtained Young's modulus for KB can be compared to the value presented in first chapter's Table 6 (150 GPa). Young's modulus of KB is inferior to the one reported for mullite which not only reflects the porosity still present but also the fact that the material is not totally constituted of mullite. Porosity influences the material's Young Modulus (E): the bigger the porosity fraction, the lower the Young's modulus [18]. The relation between the two properties is expressed by Equation 17,

$$E = E_0\,(1 - 1.9P + 0.9P^2) \qquad \textbf{Equation 17}$$

where E_0 is the Young's modulus of the dense material and P is the volume fraction porosity. The decrease of E with the increase of P is due to two main reasons: the cross-sectional area where force is applied is reduced by the presence of pores; and pores act as stress concentrators [18].

For the same type of material, mechanical properties of bulk samples and films are different. The structure, the geometry of the films and the stresses induced by the presence of the substrate are the main factors affecting their mechanical response. Since one of the dimensions of a film is much smaller than the other two, a dependence of the mechanical properties on the substrate is often observed. It is therefore very important to avoid the measurements on depths higher than 10 % of the films thickness. The structural arrangement of films is often anisotropic because grains tend to grow with differently on different directions. This leads to different properties of the grains themselves and to different interactions between them which inevitably means different mechanical properties. When a film is deposited on a substrate, it is prone to mechanical stresses. These stresses may appear due to the difference between the thermal expansion coefficients of the substrate and the films which are critical while heating and or cooling. These stresses can cause deformations which compromise the mechanical properties and the adherence of the film [47].

4 Conclusions and further work

During the development of the presented work, the main achievement was the establishment of the appropriate conditions to successfully produce kaolin thick films by EPD. Kaolin films were deposited on three types of substrate: stainless steel, platinum foil and platinized silicon. Two different sintering temperatures (1200 and 1300 ^{o}C) were tested. Kaolin green films with around 5 mg were produced regardless of the used substrate.

The production of kaolin films was only possible after a systematic characterization of kaolin powders and suspensions. To find out the suspension conditions allowing the EPD deposition of kaolin, systematic studies were carried out to evaluate the pH dependence of the zeta potential of aqueous and ethanolic media, the effect of iodine as additive, the time variation of the UV transmittance of the various suspensions media with and without iodine. Although a full understanding of all the parameters that rule the suspension's behaviour was not totally achieved, it was possible to conclude that the simultaneous addition of appropriate amounts of I_2 and H_2O to an ethanolic suspension medium was determinant for obtaining good quality kaolin suspensions to be used on the EPD process.

Changing the type of used substrate allowed a few problems to be solved. Using platinized silicon substrates allowed regular films to be obtained and to assess their mechanical properties. Kaolin films present an average Vickers hardness and an average Young's modulus of 300 MPa and 40 GPa, respectively. Considering the two sintering temperatures, i.e 1200 and 1300 ^{o}C, no major differences on the mechanical response of the films were found. KF_{1300} presents a more densified structure, as confirmed by SEM micrographs and by its lower thickness. Accordingly, the mechanical response of KF_{1300} was expected to exceed that of KF_{1200}. However, this could not be confirmed by the results of the nanoindentation tests probably due to a certain uncertainty that affects the nanoindentation results. In the case of kaolin bulk samples, a higher mechanical response was clearly observed for KB_{1300} relatively to KB_{1200}. During sintering, both KF and KB developed mullite as main crystalline phase. This is an indicator of enhanced mechanical response since mullite presents an interesting set of properties amongst them mechanical properties. In fact, the Young's modulus of KB_{1300} is not far from the literature Young's modulus of mullite. Mechanical response of kaolin films is, as expected, much different from the mechanical response of kaolin bulk samples but no equivalent data were found on the literature for comparison purposes.

SEM micrographs of the films showed that most of the kaolin particles tend to align with their basal planes parallel to the substrate. It is known that textured microstructures may present anisotropic properties and it is therefore very likely that the preferential orientation of the particles have an influence on the mechanical properties of the films. However, the possible relation between the two remains to be exploited.

Although this work allowed to exploit suitable conditions for EPD of kaolin, many aspects are yet to be explored and or understood. Regarding the suspensions stability, it is still important to develop the understanding of the effect of adding a small fraction of water to the ethanol suspension medium as, during this work, EPD of kaolin only resulted under these conditions. The complete understanding of the phenomena is probably also necessary to improve the suspensions stability, afterwards. The number of tested parameters was limited so it would also be of interest to:

- Test EPD of different types of kaolin;
- Test the effect of other additives;
- Develop a method that allows EPD on aqueous suspension media;
- Test new EPD conditions such as: different concentrations of kaolin; higher voltages; application of magnetic field;
- Test other sintering temperatures and times.

Regarding the characterization of the films, it would be of interest to quantify the exact degree of orientation of their particles and to determine the type of mullite that is formed. The type of used substrate also affects the properties of the films and further studies regarding this aspect are also of interest. Other than mechanical properties, different properties should also be determined in the future. Finding an application for these films is only possible after determining a good set of properties.

From an industrial point of view, not only the development of EPD on aqueous suspensions but also the production of good quality sintered films on less expensive substrates would be very important. To really conclude this topic, a long set of tasks is still necessary. Nevertheless, this works is a starting point to produce optimised kaolin thick films and coatings.

5 Bibliography

[1] M. F. De Riccardis, “Ceramic Coatings Obtained by Electrophoretic Deposition: Fundamentals, Models, Post-Deposition Processes and Applications,” in *Ceramic Coatings - Applications in Engineering*, InTech, 2012, pp. 43–67.

[2] I. Corni, M. P. Ryan, and A. R. Boccaccini, “Electrophoretic deposition: From traditional ceramics to nanotechnology,” *J. Eur. Ceram. Soc.*, vol. 28, no. 7, 2008.

[3] L. Besra and M. Liu, “A review on fundamentals and applications of electrophoretic deposition (EPD),” *Prog. Mater. Sci.*, vol. 52, no. 1, pp. 1–61, 2007.

[4] M. Zarbov, D. Brandon, N. Cohen, and L. Shemesh, “Engineering performance in applied EPD: Problems and solutions,” *J. Mater. Sci.*, vol. 41, no. 24, pp. 8115–8122, 2006.

[5] P. M. Vilarinho, Z. Fu, A. Wu, and A. I. Kingon, “Critical Role of Suspension Media in Electrophoretic Deposition: The Example of Low Loss Dielectric BaNd 2 Ti 5 O 14 Thick Films,” *J. Phys. Chemestry*, vol. 117, pp. 1670–1679, 2013.

[6] C. A. Piccinini, S. R. Bragança, and C. P. Bergmann, “Method for the characterization of electrophoretic properties of clay slips,” *Appl. Clay Sci.*, vol. 86, pp. 11–17, 2013.

[7] Heavens S. N., “Electrophoretic Deposition as a Processing Route for Ceramics,” *Advanced Ceramic Processing and Technology. Noyes Publications*, vol. 1, New Jersey, pp. 255–283, 1990.

[8] M. Zarbov, I. Schuster, and L. Gal-Or, “Methodology for selection of charging agents for electrophoretic deposition of ceramic particles,” *J. Mater. Sci.*, vol. 39, no. 3, pp. 813–817, 2004.

[9] B. Ferrari and R. Moreno, “Electrophoretic deposition of aqueous alumina slips,” *J. Eur. Ceram. Soc.*, vol. 17, no. 4, pp. 549–556, 1997.

[10] H. C. Hamaker, “Formation of a Deposit by Electrophoresis,” *Trans. Farad. Soc*, vol. 0, pp. 279–87, 1940.

[11] S. Cabanas-Polo and A. R. Boccaccini, “Electrophoretic deposition of nanoscale TiO2: Technology and applications,” *J. Eur. Ceram. Soc.*, vol. 36, pp. 265–283, 2016.

[12] A. Mahajan, R. Pinho, M. Dolhen, M. E. Costa, and P. M. Vilarinho, “Unleashing the Full Sustainable Potential of Thick Films of Lead-Free Potassium Sodium Niobate (K0.5Na0.5NbO3) by Aqueous Electrophoretic Deposition,” *Langmuir*, vol. 32, no. 21, pp. 5241–5249, 2016.

[13] L. Jia, Z. Lü, X. Huang, Z. Liu, K. Chen, X. Sha, G. Li, and W. Su, “Preparation of YSZ film by EPD and its application in SOFCs,” *J. Alloys Compd.*, vol. 424, no. 1–2, pp. 299–303, 2006.

[14] C. Argirusis, T. Damjanović, and G. Borchardt, “Electrophoretic deposition of thin SOFC-electrolyte films on porous La 0.75Sr0.2MnO3-δ cathodes,” *Mater. Sci. Forum*, vol. 453–454, pp. 335–342, 2004.

[15] S. T. Aruna and K. S. Rajam, “A study on the electrophoretic deposition of 8YSZ coating using mixture of acetone and ethanol solvents,” *Mater. Chem. Phys.*, vol. 111, no. 1, pp. 131–136, 2008.

[16] M. Ahmadi and H. Aghajani, “Suspension characterization and electrophoretic deposition of Yttria-stabilized Zirconia nanoparticles on an iron-nickel based superalloy,” *Ceram. Int.*, vol. 43, no. 9, pp. 7321–7328, 2017.

[17] N. Koura, T. Tsukamoto, H. Shoji, and T. Hotta, “Preparation of Various Oxide Films by an Electrophoretic Deposition Method : A Study of the Mechanism,” *J. Appl. Phys.*, vol. 34, pp. 1643–1647, 1995.

[18] W. D. Callister Jr. and D. G. Rethwisch, *Materials Science and Engineering an Introduction*, 8th ed. New York: John Wiley & Sons, Inc, 2009.

[19] M. S. Prasad, K. J. Reid, and H. H. Murray, “Kaolin: processing, properties and applications,” *Appl. Clay Sci.*, vol. 6, pp. 87–119, 1991.

[20] T. Preocanin, A. Abdelmonem, G. Montavon, and J. Luetzenkirchen, “Charging Behavior of Clays and Clay Minerals in Aqueous Electrolyte Solutions — Experimental Methods for Measuring the Charge and Interpreting the Results,” in *Clays, Clay Minerals and Ceramic Materials Bases on Clay Minerals*, InTech, pp. 51–88.

[21] R. J. Pruett, “Kaolin deposits and their uses: Northern Brazil and Georgia, USA,” *Appl. Clay Sci.*, vol. 131, pp. 3–13, 2016.

[22] P.-I. Au, P. Clode, R. S. C. Smart, and Y.-K. Leong, “Surface chemistry-microstructure-rheology of high and low crystallinity KGa-1b and KGa-2 kaolinite suspensions,” *Colloids Surfaces A Physicochem. Eng. Asp.*, vol. 484, pp. 354–364, 2015.

[23] I. Stubna, P. Sín, A. Trnik, and R. Vienthal, “Mechanical Properties of Kaolin during Heating,” *Key Eng. Mater.*, no. November, 2012.

[24] A. K. Chakraborty, *Phase Transformation of Kaolinite Clay*, 1st ed. New Delhi, 2014.

[25] M. K. R. Konduri and P. Fatehi, “Dispersion of kaolin particles with carboxymethylated xylan,” *Appl. Clay Sci.*, vol. 137, pp. 183–191, 2017.

[26] J. Yuan, W. L. Garforth, and R. J. Pruett, “Influence of dispersants on the solubility of calcined

kaolin," *Appl. Clay Sci.*, vol. 13, no. 2, pp. 137–147, 1998.

[27] F. S. Éntelis and M. E. Sheinina, "Electrophoretic forming of porcelain articles," *Glas. Ceram.(USSR)*, vol. 36, pp. 634–637, 1979.

[28] H. Schneider, J. Schreuer, and B. Hildmann, "Structure and properties of mullite-A review," *J. Eur. Ceram. Soc.*, vol. 28, no. 2, pp. 329–344, 2008.

[29] J. Martín-Márquez, J. M. Rincón, and M. Romero, "Mullite development on firing in porcelain stoneware bodies," *J. Eur. Ceram. Soc.*, vol. 30, no. 7, pp. 1599–1607, 2010.

[30] "Mullite." [Online]. Available: http://www.matweb.com/search/DataSheet.aspx?MatGUID=6ff3fda0bf744c93b4e423806faec494&ckck=1. [Accessed: 10-Aug-2017].

[31] S. P. Chaudhuri, "Ceramic Properties of Hard Porcelain in Relation to Mineralogical Composition and Microstructure: IV—Thermal-shock Resistance and Thermal Expansion," *Trans. Indian Ceram. Soc.*, vol. 34, no. 2, pp. 30–34, 1975.

[32] K. Rissa, T. Lepistö, and K. Yrjölä, "Effect of kaolin content on structure and functional properties of water-based coatings," *Prog. Org. Coatings*, vol. 55, no. 2, pp. 137–141, 2006.

[33] K. Boussois, N. Tessier-Doyen, and P. Blanchart, "High-toughness silicate ceramic," *J. Eur. Ceram. Soc.*, vol. 34, no. 1, pp. 119–126, 2014.

[34] M. H. Zimmerman, D. M. Baskin, K. T. Faber, E. R. Fuller, A. J. Allen, and D. T. Keane, "Fracture of a textured anisotropic ceramic," *Acta Mater.*, vol. 49, pp. 3231–3242, 2001.

[35] S. Deniel, N. Tessier-Doyen, C. Dublanche-Tixier, D. Chateigner, and P. Blanchart, "Processing and characterization of textured mullite ceramics from phyllosilicates," *J. Eur. Ceram. Soc.*, vol. 30, no. 12, pp. 2427–2434, 2010.

[36] D. Antal, T. Húlan, I. Štubňa, M. Záleská, and A. Trník, "The influence of texture on elastic and thermophysical properties of kaolin- and illite-based ceramic bodies," *Ceram. Int.*, vol. 43, pp. 2730–2736, 2016.

[37] M. De Graef and M. E. McHenry, *STRUCTURE OF MATERIALS An Introduction to Crystallographt, diffraction, and Symmetry*. Cambridge: Cambridge University Press, 2007.

[38] R. L. Snyder, "The Use of Reference Intensity Ratios in X-Ray Quantitative Analysis," *Powder Diffr.*, vol. 7, pp. 186–193, 1992.

[39] P. Gallagher, *Handbook of thermal analysis and calorimetry*, 1st ed. Ohio: Elsevier, 1998.

[40] K. Khoshnevisan and M. Barkhi, "Zeta potential," Tehran, Institute of Agricultural Biotechnologyy, Nano Department, 2015.

[41] M. G. Gore, *Spectrophotometry and Spectrofluorimetry: Practical Approach*, 1st ed.

Southampton: Oxford University Press, 2000.

[42] “Laser diffraction particle sizing technique.” [Online]. Available: https://www.malvern.com/en/products/technology/laser-diffraction. [Accessed: 22-Jul-2017].

[43] F. Rouquerol, J. Rouquerol, and K. Sing, *Adsorption by Powders and Porous Solids Principles, Methodology and Applications*, 1st ed. Marseille: Academic Press, 1998.

[44] W. C. Oliver and G. M. Pharr, “Measurement of hardness and elastic modulus by instrumented indentation: Advances in understanding and refinements to methodology,” *J. Mater. Res.*, vol. 19, no. 1, pp. 3–20, 2004.

[45] C. Instruments, “Indentation Software User ’ s manual.” CSM Instruments SA, Peseux (Switzerland), 2008.

[46] T. A. C. Society, “Structure and Properties of Ceramics.” [Online]. Available: http://ceramics.org/learn-about-ceramics/structure-and-properties-of-ceramics. [Accessed: 06-Oct-2017].

[47] F. Richter, “Mechanical properties of solid bulk materials and thin films - A Lecture Series for the Teaching Programme of the International Research Training Group ‘Materials and Concepts for Advanced Interconnects,’” Chemnitz, 2010.